JCI The Journal of Clinical Investigation

CCL28-induced RARβ expression inhibits oral squamous cell carcinoma bone invasion

Junhee Park, … , Kwang-Kyun Park, Won-Yoon Chung

J Clin Invest. 2019;129(12):5381-5399. https://doi.org/10.1172/JCI125336.

Research Article **Oncology**

Oral squamous cell carcinoma (OSCC) frequently invades the maxillary or mandibular bone, and this bone invasion is closely associated with poor prognosis and survival. Here, we show that CCL28 functions as a negative regulator of OSCC bone invasion. CCL28 inhibited invasion and epithelial-mesenchymal transition (EMT), and its inhibition of EMT was characterized by induced E-cadherin expression and reduced nuclear localization of β-catenin in OSCC cells with detectable RUNX3 expression levels. CCL28 signaling via CCR10 increased retinoic acid receptor-β (RARβ) expression by reducing the interaction between RARα and HDAC1. In addition, CCL28 reduced RANKL production in OSCC and osteoblastic cells and blocked RANKL-induced osteoclastogenesis in osteoclast precursors. Intraperitoneally administered CCL28 inhibited tumor growth and osteolysis in mouse calvaria and tibia inoculated with OSCC cells. RARβ expression was also increased in tumor tissues. In patients with OSCC, low CCL28, CCR10, and RARβ expression levels were highly correlated with bone invasion. Patients with OSCC who had higher expression of CCL28, CCR10, or RARβ had significantly better overall survival. These findings suggest that CCL28, CCR10, and RARβ are useful markers for the prediction and treatment of OSCC bone invasion. Furthermore, CCL28 upregulation in OSCC cells or CCL28 treatment can be a therapeutic strategy for OSCC bone invasion.

Find the latest version:

https://jci.me/125336/pdf

CCL28-induced RARβ expression inhibits oral squamous cell carcinoma bone invasion

Junhee Park,[1,2,3] Xianglan Zhang,[4,5] Sun Kyoung Lee,[2,3] Na-Young Song,[1,3] Seung Hwa Son,[4] Ki Rim Kim,[6] Jae Hoon Shim,[2] Kwang-Kyun Park,[1,2,3] and Won-Yoon Chung[1,2,3,4]

[1]Department of Dentistry and [2]Department of Applied Life Science, Graduate School, Yonsei University, Seoul, Korea. [3]Department of Oral Biology and BK21 PLUS project, Yonsei University College of Dentistry, Seoul, Korea. [4]Oral Cancer Research Institute, Yonsei University College of Dentistry, Seoul, Korea. [5]Department of Pathology, Yanbian University Hospital, Yanji city, China. [6]Department of Dental Hygiene, College of Science and Engineering, Kyungpook National University, Sangju, Korea.

Oral squamous cell carcinoma (OSCC) frequently invades the maxillary or mandibular bone, and this bone invasion is closely associated with poor prognosis and survival. Here, we show that CCL28 functions as a negative regulator of OSCC bone invasion. CCL28 inhibited invasion and epithelial-mesenchymal transition (EMT), and its inhibition of EMT was characterized by induced E-cadherin expression and reduced nuclear localization of β-catenin in OSCC cells with detectable RUNX3 expression levels. CCL28 signaling via CCR10 increased retinoic acid receptor-β (RARβ) expression by reducing the interaction between RARα and HDAC1. In addition, CCL28 reduced RANKL production in OSCC and osteoblastic cells and blocked RANKL-induced osteoclastogenesis in osteoclast precursors. Intraperitoneally administered CCL28 inhibited tumor growth and osteolysis in mouse calvaria and tibia inoculated with OSCC cells. RARβ expression was also increased in tumor tissues. In patients with OSCC, low CCL28, CCR10, and RARβ expression levels were highly correlated with bone invasion. Patients with OSCC who had higher expression of CCL28, CCR10, or RARβ had significantly better overall survival. These findings suggest that CCL28, CCR10, and RARβ are useful markers for the prediction and treatment of OSCC bone invasion. Furthermore, CCL28 upregulation in OSCC cells or CCL28 treatment can be a therapeutic strategy for OSCC bone invasion.

Introduction

Oral squamous cell carcinoma (OSCC), which accounts for 40% of all head and neck squamous cell carcinoma (HNSCC) cases, not only frequently metastasizes to distant sites but also invades the maxillary or mandibular bone based on its anatomically close proximity to the jaw bone (1, 2). Bone invasion is a frequent complication of OSCC and dramatically impacts patient recovery and quality of life by causing high recurrence, significant morbidity, and poor prognosis (3, 4). Therefore, more accurate prediction and early detection of bone invasion in patients with OSCC are required for planning appropriate treatment and disease control.

Bone invasion of cancer cells, including OSCC cells, produces severe osteolytic lesions due to interactions between the tumor and the bone microenvironment or stromal cells at the invasive front (5). OSCC cells close to the bone surface invade bones via epithelial-mesenchymal transition (EMT) and by degrading the bone matrix with proteolytic enzymes. The invading tumor cells change the bone microenvironment by secreting TNF-α, interleukins, parathyroid hormone–related protein (PTHrP), and chemokines, which activate osteoclasts directly and/or stimulate RANKL expression in stromal stem cells and osteoblasts (6, 7). The resorption of bone matrix by mature osteoclasts releases bone-storing growth factors. In particular, TGF-β has been reported to stimulate the production of osteolytic factors and invasion to jaw bone by promoting EMT in OSCC cells (8–10).

Chemokines are soluble factors secreted from various cell types in response to cytokines and growth factors and control autocrine and paracrine communications via their receptors. Most chemokines secreted by tumors and surrounding stromal cells at primary tumor sites or premetastatic niches have been recognized to contribute to the survival, acquisition of invasive phenotypes, and metastatic tropism of tumor cells (11–13). Several chemokines derived from bone-tropic tumor cells act as osteolytic factors by inducing bone resorption of osteoclasts and promoting the recruitment and differentiation of osteoclast precursors (14–16), and the levels of these chemokines in serum or bone marrow are associated with cancer-mediated osteolysis in humans (17, 18). In the case of OSCC, various chemokines, including CXCL12/CXCR4, CCL5/CCR5, CXCL8, and CCL2, are known to play critical roles in invasion and metastasis by promoting EMT, MMP expression, and cell dissemination (19–21). OSCC cell–derived CXCL2 and CXCL13 induce RANKL expression in osteoblastic/stromal cells (22, 23), and serum levels of CXCL9 and tissue expression of CCL2 are positively correlated with OSCC bone invasion (24, 25). However, more studies are required to identify chemokines to determine the bone-invasive potential of OSCC and targeted therapy for bone invasion in OSCC.

We previously reported the distinct roles of RUNX3 expression in bone destruction caused by different types of cancer. RUNX3 inhibited lung cancer cell–mediated bone destruction and blocked cancer cell invasion and osteoclastogenesis by downregulating CCL5 and upregulating CCL19 and CXCL11 (26). In con-

Conflict of interest: The authors have declared that no conflict of interest exists.
Copyright: © 2019, American Society for Clinical Investigation.
Submitted: October 12, 2018; **Accepted:** September 3, 2019; **Published:** November 4, 2019.
Reference information: *J Clin Invest*. 2019;129(12):5381–5399.
https://doi.org/10.1172/JCI125336.

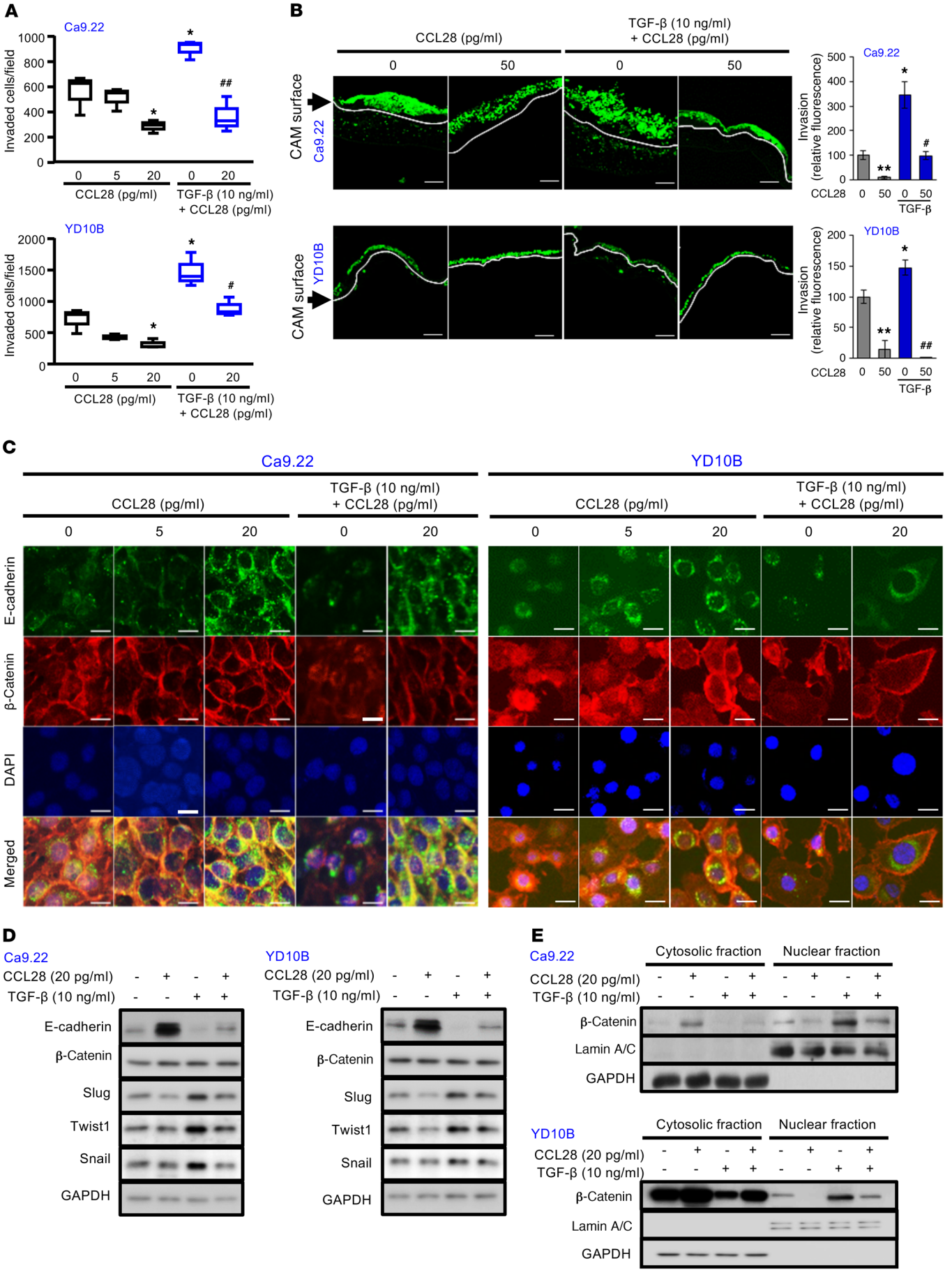
A
Ca9.22
Invaded cells/field
CCL28 (pg/ml)
TGF-β (10 ng/ml) + CCL28 (pg/ml)
YD10B
B
CCL28 (pg/ml)
TGF-β (10 ng/ml) + CCL28 (pg/ml)
CAM surface
Ca9.22
YD10B
Invasion (relative fluorescence)
C
Ca9.22
YD10B
E-cadherin
β-Catenin
DAPI
Merged
D
Ca9.22
YD10B
CCL28 (20 pg/ml)
TGF-β (10 ng/ml)
E-cadherin
β-Catenin
Slug
Twist1
Snail
GAPDH
E
Cytosolic fraction
Nuclear fraction
Lamin A/C

Figure 1. CCL28 inhibits invasion and EMT in OSCC cells. (**A**) Invasion of Ca9.22 and YD10B OSCC cells treated with CCL28 and/or TGF-β (mean ± SEM, $n = 3$). $^{*}P < 0.05$ vs. cells without CCL28 and TGF-β; $^{\#}P < 0.05$, $^{\#\#}P < 0.005$ vs. TGF-β–only–treated cells by 1-way ANOVA with multiple-comparisons test. (**B**) Invasion of Ca9.22 and YD10B OSCC cells with CCL28 and/or TGF-β into the CAMs of fertilized eggs (mean ± SEM, $n = 3$). Representative images of CAM. Scale bars: 100 μm. Cells invaded into the mesoderm layer of CAMs are quantified by the mean fluorescence. $^{*}P < 0.05$, $^{**}P < 0.01$ vs. cells without CCL28 and TGF-β; $^{\#}P < 0.05$, $^{\#\#}P < 0.001$ vs. TGF-β–only–treated cells by 1-way ANOVA with multiple-comparisons test. (**C**) Expression levels and cellular localization of E-cadherin and β-catenin in Ca9.22 and YD10B OSCC cells treated with CCL28 and/or TGF-β. Representative immunofluorescence images. Scale bars: 100 μm. (**D**) Expression levels of E-cadherin, β-catenin, and EMT-regulating transcription factors in Ca9.22 and YD10B OSCC cells treated with CCL28 and/or TGF-β. (**E**) Cytosolic and nuclear β-catenin levels in Ca9.22 and YD10B OSCC cells treated with CCL28 and/or TGF-β. (**D** and **E**) Representative Western blot images.

trast, RUNX3 promoted bone invasion of OSCC cells by inducing EMT and PTHrP expression (27). In the present study, we found that CCL28 is regulated by RUNX3. CCL28 inhibited the invasiveness of OSCC cells by inducing retinoic acid receptor-β (RARβ) via its receptor CCR10 and preventing RANKL expression in OSCC and osteoblastic cells and RANKL-induced differentiation of osteoclast precursors. We further evaluated whether the CCL28/CCR10/RARβ axis is involved in bone invasion using murine models and tumor tissues of patients with OSCC. To our knowledge, this is the first report verifying the role of CCL28 in cancer cell–mediated bone destruction.

Results

CCL28 treatment inhibits invasion and EMT in OSCC cells. To identify novel markers driving bone invasion of OSCC cells, using RT^2 Profiler PCR Arrays, we first investigated chemokines regulated by RUNX3, proven to play a critical role in bone invasion of OSCC in our previous study (27). Among 89 chemokines, CCL28 mRNA expression was significantly upregulated in RUNX3-knockdown Ca9.22 gingival SCC cells (Supplemental Table 1; supplemental material available online with this article; https://doi.org/10.1172/JCI125336DS1). Increased CCL28 protein levels were also confirmed in RUNX3-knockdown Ca9.22 and YD10B OSCC cells (Supplemental Figure 1A) and in the tumor tissues of RUNX3-knockdown Ca9.22 cell–injected mice obtained from our previous study (Supplemental Figure 1B). Our finding that CCL28 expression is regulated by RUNX3 was further verified by the downregulated CCL28 expression in OSCC cells with increased RUNX3 expression (Supplemental Figure 1C). The expression of CCL28 and its receptors, CCR3 and CCR10 (Supplemental Figure 2A), and the secretion of CCL28 (Supplemental Figure 2B) were detected in RUNX3-expressing Ca9.22 and YD10B and RUNX3-nonexpressing HSC2 and HSC3 OSCC cells. However, CCL28 treatment did not affect cell viability (Supplemental Figure 2C) and induce apoptotic and necrotic cell death (Supplemental Figure 2D) in OSCC cell lines. Interestingly, the invasion of Ca9.22 and YD10B cells was markedly inhibited by CCL28 treatment in the absence or presence of TGF-β, one of the abundantly stored growth factors in the bone matrix that is released by osteoclastic bone resorption (Figure 1A), whereas the invasion of RUNX3-nonexpressing HSC2 and HSC3 cells was not (Supplemental Figure 3A). In addition, CCL28 treatment inhibited the invasion promoted by RUNX3 overexpression in RUNX3-expressing Ca9.22 and YD10B cells but did not inhibit the invasion promoted by RUNX3 expression in RUNX3-nonexpressing HSC2 and HSC3 cells (Supplemental Figure 3B). In chicken chorioallantoic membrane (CAM) invasion assays using fluorescently labeled OSCC cells, CCL28 treatment reduced the number of Ca9.22 and YD10B cells invading below the CAM surface in the absence or presence of TGF-β (Figure 1B).

EMT is a developmental process that promotes the switching of tumor cells from an epithelial phenotype to a mesenchymal phenotype with invasive properties (28). Loss of E-cadherin and accumulation of β-catenin in the nucleus are considered fundamental hallmarks of EMT. TGF-β, a typical EMT inducer in cancer cells, reduces E-cadherin expression required for cell-cell adhesion and stimulates the nuclear localization of β-catenin for the transcription of EMT-related target genes (29, 30). Confocal imaging (Figure 1C) and Western blot analysis (Figure 1D) indicated that CCL28 treatment increased E-cadherin expression and blocked the downregulation of E-cadherin by TGF-β stimulation in Ca9.22 and YD10B OSCC cells. Furthermore, CCL28 treatment downregulated the EMT-related transcription factors Slug, Twist, and/or Snail (Figure 1D) and inhibited the translocation of β-catenin from the cytoplasm to the nucleus (Figure 1E) in both OSCC cell lines in the absence or presence of TGF-β. These results indicate that CCL28 expression is downregulated by RUNX3 in RUNX3-expressing OSCC cells, although CCL28 is expressed in all OSCC cells, and that CCL28 treatment inhibits cell invasion and EMT in RUNX3-expressing OSCC cells.

The CCL28/CCR10 axis inhibits OSCC cell invasion and is associated with oral carcinogenesis. Next, we investigated whether the blockade of CCL28 expression in Ca9.22 and YD10B OSCC cells could affect their invasion. Invasion was noticeably enhanced in Ca9.22 and YD10B cell lines transduced with CCL28-specific shRNAs compared with that in control cells transduced with corresponding nonspecific scrambled shRNAs but was inhibited by CCL28 treatment (Figure 2A). CCL28 is known as a functional ligand for CCR3 and CCR10 (31). We established CCR3- or CCR10-knockdown cells using Ca9.22 and YD10B OSCC cell lines and specific shRNA-containing lentiviral particles. OSCC cell invasion was not affected by CCR3 (Figure 2B) or CCR10 knockdown (Figure 2C). CCL28 treatment did not inhibit the invasion of CCR10-knockdown OSCC cells but still inhibited that of CCR3-knockdown cells. The results of CAM invasion assays supported the in vitro effect of CCL28 or CCR10 knockdown on the invasion of OSCC cells in the absence or presence of CCL28 (Figure 2D). These results suggest that the reduced CCL28 expression promotes the invasion of Ca9.22 and YD10B OSCC cells and that the release of CCL28 into the tumor microenvironment from OSCC cells and surrounding stromal cells can transmit the CCL28 signal into OSCC cells via CCR10, thereby inhibiting the invasion of Ca9.22 and YD10B OSCC cells.

Clinical data from The Cancer Genome Atlas (TCGA) database showed that compared with that in adjacent normal tissues, CCL28 gene expression was significantly downregulated in HNSCC tissues, whereas the gene expression of its receptors CCR3 and CCR10 was not significantly different (Figure 2E).

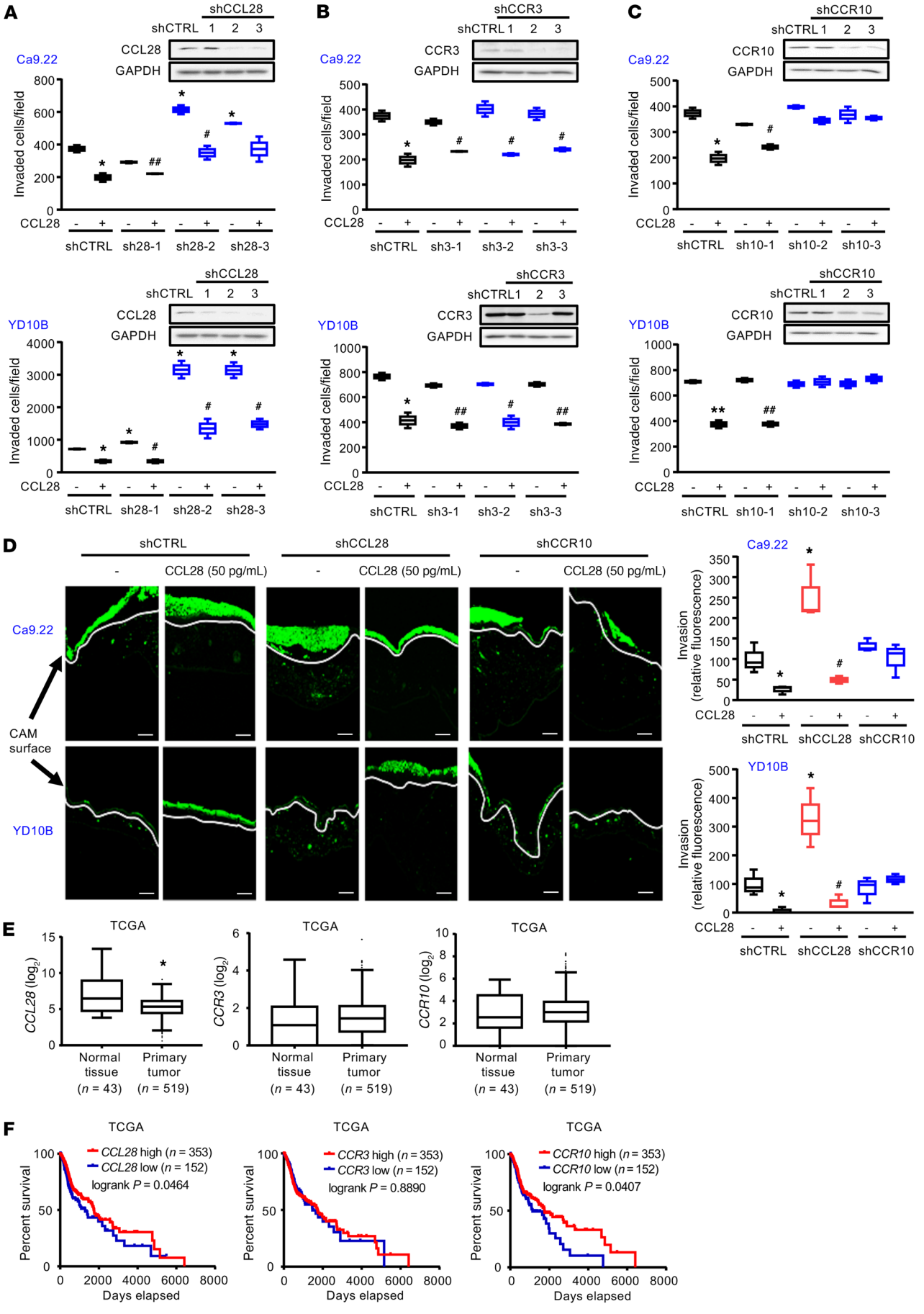
A
shCCL28
shCTRL 1 2 3
CCL28
GAPDH
Ca9.22
Invaded cells/field
CCL28
shCTRL sh28-1 sh28-2 sh28-3
YD10B
B
shCCR3
CCR3
shCTRL 1 2 3
shCTRL sh3-1 sh3-2 sh3-3
C
shCCR10
CCR10
shCTRL sh10-1 sh10-2 sh10-3
D
shCTRL
shCCL28
shCCR10
- CCL28 (50 pg/mL)
CAM surface
Invasion (relative fluorescence)
E
TCGA
CCL28 (log2)
CCR3 (log2)
CCR10 (log2)
Normal tissue (n = 43)
Primary tumor (n = 519)
F
CCL28 high (n = 353)
CCL28 low (n = 152)
logrank P = 0.0464
CCR3 high (n = 353)
CCR3 low (n = 152)
logrank P = 0.8890
CCR10 high (n = 353)
CCR10 low (n = 152)
logrank P = 0.0407
Percent survival
Days elapsed

Figure 2. CCL28 inhibits OSCC cell invasion via CCR10 and is associated with carcinogenesis and survival in patients. (**A**) Invasion of CCL28-knockdown OSCC cells. (**B**) Invasion of CCR3-knockdown OSCC cells. (**C**) Invasion of CCR10-knockdown OSCC cells. (**A**–**C**) OSCC cells were transduced with lentiviral particles with control shRNAs or 3 different shRNAs targeting CCL28, CCR10, or CCR3. Knockdown of CCL28, CCR10, or CCR3 in transduced cells was confirmed by Western blotting (top panels). Cell invasion is quantified as the number of invaded cells per field (mean ± SEM, $n = 3$). $^{*}P < 0.05$, $^{**}P < 0.005$ vs. control shRNA–transfected cells without CCL28; $^{\#}P < 0.05$, $^{\#\#}P < 0.01$ vs. CCL28-, CCR3-, or CCR10-specific shRNA–transfected cells without CCL28 by 1-way ANOVA with multiple-comparisons test. (**D**) Invasion of CCL28- or CCR10-knockdown OSCC cells labeled with CFDA-SE and then suspended in a DMEM/Matrigel (4:1) mixture on the CAMs of fertilized eggs (mean ± SEM, $n = 3$). Representative images of CAM. Scale bars: 100 μm. Cells invaded into the mesoderm layer are quantified by the mean fluorescence. $^{*}P < 0.05$ versus control shRNA–transfected cells without CCL28; $^{\#}P < 0.01$ vs. CCL28- or CCR10-knockdown cells without CCL28 by 1-way ANOVA with multiple-comparisons test. (**E**) CCL28, CCR3, or CCR10 mRNA levels in normal and HNSCC tissues. The data were obtained from the TCGA database. Box plots show the median and interquartile range. $^{*}P < 0.0001$ vs. normal tissue by 2-tailed Student's t test. (**F**) Kaplan-Meier survival curves for HNSCC patients with high or low expression of CCL28, CCR3, or CCR10 mRNA by the log-rank test.

Additionally, the overall survival of HNSCC patients with higher gene expression of CCL28 or CCR10, but not CCR3, was increased (Figure 2F). These results indicate that CCL28 and CCR10 are associated with carcinogenesis and prognosis in HNSCC patients.

CCL28 inhibits OSCC cell invasion by stimulating RARE-related transcriptional activity via CCR10 and upregulated RARβ expression. To determine the molecular mechanism underlying the anti-invasive activity of CCL28 via CCR10, we measured the activities of 45 pathways in Ca9.22 and YD10B OSCC cells and their CCR10-knockdown counterparts using Cignal Finder Reporter Arrays and described the expression levels of reporter genes as fold changes in CCL28-treated OSCC cells versus CCL28-untreated cells and in CCL28-treated CCR10-knockdown cells versus CCL28-untreated CCR10-knockdown cells. Interestingly, the expression of the reporter gene associated with retinoic acid response elements (RAREs) was enhanced by CCL28 treatment in Ca9.22 and YD10B cells but not by CCL28 treatment in CCR10-knockdown OSCC cells (Figure 3A). In the presence of endogenous retinoic acid (RA), the binding of RAR/retinoid X receptor (RXR) heterodimers to RAREs mediates the transcription of primary RA target genes, including *RARB*. RARβ, particularly its isoform RARβ2, has been shown to suppress tumors by inducing cell cycle arrest, differentiation, and apoptosis, and the silencing of RARβ and RARβ2 has been correlated with tumor grade in human cancers (32, 33). Analysis of TCGA HNSCC data set showed that CCL28 gene expression was significantly correlated with the expression of the RARβ gene and the RA signature corresponding to the sum of expression values of the genes that are regulated by agonists of RARs (Figure 3B). We confirmed that CCL28 treatment upregulated RARβ and RARβ2 protein expression in Ca9.22 and YD10B OSCC cells but not in HSC2 and HSC3 cells (Figure 3C). RARβ and RARβ2 protein expression was upregulated in CCL28-overexpressing Ca9.22 and YD10B OSCC cells and downregulated in CCL28-knockdown cells (Figure 3D). The upregulation of RARβ by CCL28 treatment was abrogated by CCR10 knockdown but not by CCR3 knockdown (Figure 3E). Treatment with the RARβ-selective antagonist LE135 or the inverse pan-RAR agonist BMS493 blocked CCL28-mediated inhibition of invasion in Ca9.22 and YD10B OSCC cells (Figure 3F). These results indicate that CCL28/CCR10 signaling inhibits OSCC cell invasion by inducing RARβ, particularly RARβ2, expression via RARE-related transcriptional activation.

CCL28 induces RAR expression by decreasing RARα-HDAC1 interaction. Upon the binding of ligands, RARα controls the expression of RARβ at the transcriptional level (34). Thus, we determined whether RARβ expression could also be regulated by RARα in CCL28-treated Ca9.22 and YD10B OSCC cells. The protein level of RARα was elevated by CCL28 treatment as observed for RARβ and RARβ2. Treatment with a selective RARα antagonist, ER50891, blocked the upregulation of RARβ and its isoform RARβ2 in CCL28-treated OSCC cells (Figure 4A) and abrogated the inhibitory effect of CCL28 on OSCC cell invasion (Figure 4B). In addition, treatment with ER50891 or LE135 blocked the upregulation of E-cadherin and rescued the expression of EMT-related transcription factors as well as the nuclear translocation of β-catenin in CCL28-treated OSCC cells (Supplemental Figure 4). The expression of tumor suppressor genes, including *RARB*, is often inactivated by the methylation of upstream promoter regions of target genes and chromatin deacetylation in tumor cells (35). The *RARB2* promoter is methylated in two-thirds of head and neck cancers and half of oral intraepithelial neoplasia cases. In head and neck cancer cell lines with the unmethylated *RARB2* promoter, *RARB2* silencing has been suggested to be involved in histone deacetylation (36). DNA methyltransferase (DNMT) and histone deacetylase (HDAC) are recruited to the transcriptional corepressor complex interacting with RARα on RAREs, blocking the expression of RARβ at the transcriptional level. In addition, DNMT and HDAC inhibitors have been shown to reactivate RARβ (37). Based on Western blotting and IP assays, CCL28 treatment decreased the interaction between RARα and HDAC1 but not the interaction between RARα and DNMT (Figure 4C). We further investigated the acetylation of histone H3 and recruited HDAC1 levels in the RARβ promoter region of CCL28-treated OSCC cells by ChIP–quantitative PCR. Acetylated histone H3 levels were increased and HDAC1 levels were decreased by CCL28 treatment (Figure 4D). These results suggest that CCL28 upregulates RARα-mediated transcription of RARβ by reducing HDAC1-induced epigenetic changes, thereby inhibiting EMT and invasion in OSCC cells.

CCL28 inhibits RANKL expression in OSCC and osteoblastic cells and RANKL-induced differentiation in osteoclast precursors. Cancer cells causing bone loss directly secrete RANKL or stimulate RANKL production in osteoblastic/stromal cells exposed to cancer cell–derived osteolytic factors. RANKL induces osteoclastogenesis by binding to its receptor RANK on osteoclast precursors, and the differentiated osteoclasts participate in bone resorption. RANKL is counteracted by its decoy receptor osteoprotegerin (OPG). Treatment with OPG inhibits bone invasion of OSCC cells by inhibiting osteoclastogenesis and cancer cell migration (38). CCL28 treatment significantly reduced the secreted levels of RANKL from Ca9.22 and YD10B OSCC cells but did not affect those of OPG, lowering the RANKL/OPG ratio (Figure 5A). These effects of CCL28 were not detected in HSC2 or HSC3 OSCC cells

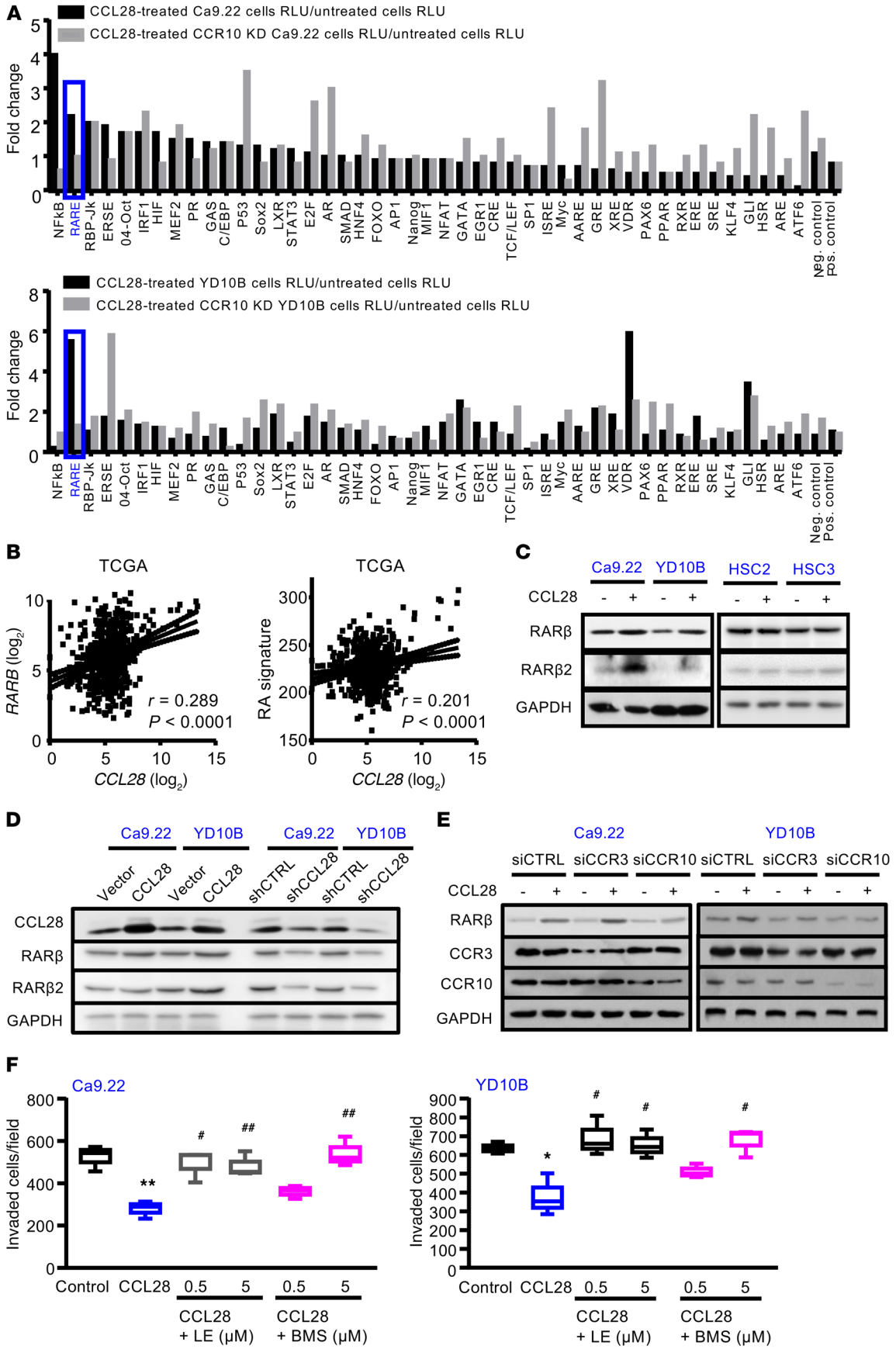
A
CCL28-treated Ca9.22 cells RLU/untreated cells RLU
CCL28-treated CCR10 KD Ca9.22 cells RLU/untreated cells RLU
Fold change
NFkB RARE RBP-Jk ERSE 04-Oct IRF1 HIF MEF2 PR GAS C/EBP P53 Sox2 LXR STAT3 E2F AR SMAD HNF4 FOXO AP1 Nanog MIF1 NFAT GATA EGR1 CRE TCF/LEF SP1 ISRE Myc AARE GRE XRE VDR PAX6 PPAR RXR ERE SRE KLF4 GLI HSR ARE ATF6 Neg. control Pos. control
CCL28-treated YD10B cells RLU/untreated cells RLU
CCL28-treated CCR10 KD YD10B cells RLU/untreated cells RLU
B
TCGA
RARB (log2)
CCL28 (log2)
r = 0.289
P < 0.0001
TCGA
RA signature
CCL28 (log2)
r = 0.201
P < 0.0001
C
Ca9.22 YD10B HSC2 HSC3
CCL28
RARβ
RARβ2
GAPDH
D
Ca9.22 YD10B Ca9.22 YD10B
Vector CCL28 Vector CCL28 shCTRL shCCL28 shCTRL shCCL28
CCL28
RARβ
RARβ2
GAPDH
E
Ca9.22 YD10B
siCTRL siCCR3 siCCR10 siCTRL siCCR3 siCCR10
CCL28
RARβ
CCR3
CCR10
GAPDH
F
Ca9.22
Invaded cells/field
Control CCL28 0.5 5 0.5 5
CCL28 + LE (μM)
CCL28 + BMS (μM)
YD10B
Invaded cells/field
Control CCL28 0.5 5 0.5 5
CCL28 + LE (μM)
CCL28 + BMS (μM)

Figure 3. The CCL28/CCR10 axis inhibits OSCC cell invasion by activating RAR signaling. (**A**) Representative pathway reporter array (n = 2) for wild-type and CCR10-knockdown (KD) OSCC cells in the absence or presence of CCL28 (20 ng/mL). Reporter gene activities in CCL28-treated cells were normalized by those in untreated cells and represented as fold changes. (**B**) Correlations between CCL28 mRNA expression and RARβ mRNA expression in patients with HNSCC by Pearson's correlation analysis. Scatter plots represent normalized RSEM values for each gene. (**C**) RARβ and RARβ2 expression in response to CCL28 treatment (20 pg/mL) in Ca9.22, YD10B, HSC2, or HSC3 OSCC cells. (**D**) RARβ and RARβ2 expression in CCL28-overexpressing or CCL28-knockdown Ca9.22 or YD10B OSCC cells. (**E**) RARβ expression in response to CCL28 treatment (20 pg/mL) in CCR3- or CCR10-downregulated Ca9.22 or YD10B OSCC cells. (**C**–**E**) Representative Western blot images. (**F**) Invasion of OSCC cells treated with the RARβ-selective antagonist LE135 or the inverse pan-RAR agonist BMS493 in the presence of CCL28 (20 pg/mL) (mean ± SEM, n = 3). $^{*}P < 0.05$ and $^{**}P < 0.005$ versus CCL28-untreated cells; $^{\#}P < 0.05$ and $^{\#\#}P < 0.01$ versus CCL28-only-treated cells by 1-way ANOVA with multiple-comparisons test.

(Supplemental Figure 5A). Treatment with the selective RARα antagonist ER50891 and the RARβ antagonist LE135 prevented the reduction in RANKL levels secreted from CCL28-treated Ca9.22 and YD10B OSCC cells (Figure 5B). In the absence of OSCC cell–conditioned media containing osteolytic factors, CCL28 treatment reduced RANKL levels but did not affect OPG levels secreted from hFOB1.19 osteoblastic cells (Figure 5C). Treatment with OSCC cell–conditioned media elevated the secreted levels of RANKL and lowered those of OPG in osteoblastic cells. However, CCL28 treatment significantly restored the RANKL/OPG ratio by blocking elevated RANKL production (Figure 5D). In addition, CCL28 treatment inhibited RANKL-induced osteoclast formation in bone marrow–derived macrophages (BMMs) as osteoclast precursors (Figure 5E). In RANKL-treated BMMs, osteoclast formation was inhibited by conditioned media of CCL28-overexpressing OSCC cells but increased by conditioned media of CCL28-knockdown OSCC cells (Supplemental Figure 5B). These results indicate that CCL28 inhibits osteoclast formation by decreasing RANKL levels in both OSCC cells and osteoblasts, as well as by directly affecting RANKL-stimulated osteoclast precursors.

CCL28 treatment inhibits OSCC-induced osteolysis in vivo. We further evaluated the in vivo activity of CCL28 using 2 murine models of cancer cell–mediated bone loss, calvarial and intratibial xenograft mouse models. In the calvarial model, subcutaneously injected cancer cells directly invade the calvarium by penetrating the basement membrane and induce osteolysis (39). Ca9.22 OSCC cells were inoculated in the calvaria of mice, and CCL28 was intraperitoneally injected 3 times per week. Indeed, tumor volume was suppressed by CCL28 administration in a dose-dependent manner and almost completely at 50 μg/kg (Figure 6A). Three-dimensional (3D) imaging (Figure 6B) and evaluation of bone volume over total volume (BV/TV) and bone surface density (BS/BV), which are bone morphometric parameters derived from micro-CT (μCT) scans (Figure 6C), showed that OSCC-induced osteolysis was significantly inhibited by CCL28 injection. Intraperitoneal administration of CCL28 at 50 μg/kg blocked the decrease in BV/TV and the increase in BS/BV by OSCC cell inoculation. CCL28 administration inhibited the serum levels of bone turnover markers, including calcium, tartrate-resistant acid phosphatase-5b (TRAP-5b), C-terminal cross-linking telopeptide of type I collagen (CTX), and alkaline phosphatase (ALP), in OSCC cell–inoculated mice (Figure 6D). H&E staining also showed that CCL28 administration inhibited tumor growth and bone invasion (Figure 6E). TRAP staining indicated a reduced number of TRAP-positive osteoclasts at the invasive front of the tumor in CCL28-treated mice compared with that in vehicle-treated mice (Figure 6, E and F). IHC analysis showed that CCL28 administration suppressed the expression of Ki67, a proliferation marker, and CD31, an endothelial cell marker, but induced the expression of RARβ (Figure 6G).

Moreover, the increased CCL28 expression in OSCC cells reduced the invasive capability of cancer cells (Supplemental Figure 6A) and mitigated osteolysis in vivo. Compared with mice inoculated with cells with empty vector, mice inoculated with CCL28-overexpressing Ca9.22 cells exhibited reduced tumor volume and osteolysis (Supplemental Figure 6, B and C), and bone morphometric parameters, BV/TV and BS/BV, were recovered to control levels (Supplemental Figure 6D).

Oral cancer can metastasize to distant bone and induce osteolysis (1, 2). Thus, we evaluated OSCC-associated bone destruction and the effect of CCL28 injection using an intratibial xenograft model. Intraperitoneally administered CCL28 inhibited the emergence of osteolytic lesions in a dose-dependent manner following injection of YD10B OSCC cells into the tibial bone marrow of mice, as shown in 3D images (Figure 7A). Moreover, CCL28 administration rescued bone morphometric parameters by significantly inhibiting the decrease in BV/TV and trabecular number (Tb.N) values and increase in trabecular separation (Tb.Sp) and the structure model index (SMI) values mediated by OSCC cell inoculation (Figure 7B). CCL28 administration also inhibited the serum levels of bone turnover markers (Figure 7C), tumor volume and bone invasion (Figure 7, D and E), the number of TRAP-positive osteoclasts on the bone surfaces near the tumors (Figure 7, D and F), and the expression of Ki67 and CD31 (Figure 7G) but induced RARβ expression. These findings demonstrate that CCL28 prevents tumor growth and osteolysis and upregulates RARβ in vivo.

Expression levels of CCL28, CCR10, and RARβ are closely associated with bone invasion and overall survival in patients with OSCC. Next, we estimated whether CCL28, CCR3, CCR10, and RARβ can serve as critical markers for OSCC bone invasion. The expression of these proteins was detected in 117 human OSCC tissues by IHC staining using specific antibodies (Figure 8A). The histoscores for the expression of CCL28, its receptors, and RARβ ranged from 1 to 100 in most normal oral mucosa, but the expression of these molecules fluctuated in oral cancer tissues (Figure 8B). Based on the histoscores, the expression of each molecule was graded as low (histoscore 0–100) or high (histoscore 101–300). CCL28 expression showed a close correlation with RARβ expression (Supplemental Table 2). The relationships between the expression of CCL28, its receptors, or RARβ and clinicopathologic characteristics in patients with OSCC are displayed in Table 1. Bone invasion was detected in 57.3% of 117 patients with OSCC and at a higher frequency than perineural and vascular invasion. Low CCL28, CCR10, and RARβ expression levels were highly correlated with bone invasion in patients with OSCC. In addition, patients with OSCC who had higher expression of CCL28, CCR10, or RARβ had significantly better overall survival, but the CCR3 expression level

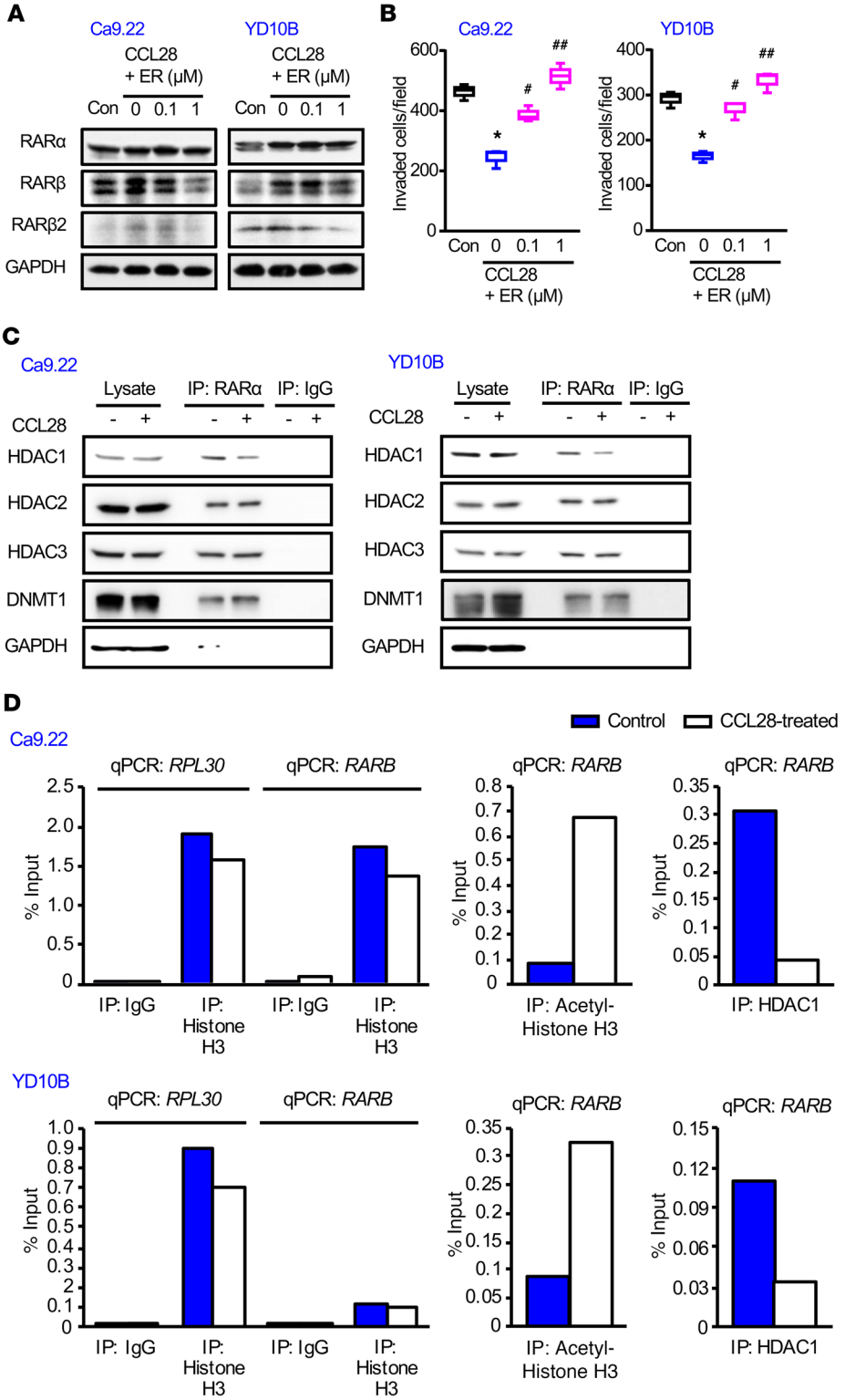

Figure 4. CCL28 upregulates RARβ expression via RARα-mediated transcription by reducing the interaction between RARα and HDAC1. (**A**) RARβ and RARβ2 expression levels in OSCC cells treated with CCL28 (20 pg/mL) and/or the selective RARα antagonist ER50891 (ER). (**B**) Invasion of OSCC cells treated with CCL28 (20 pg/mL) and/or the selective RARα antagonist ER50891 (ER) (mean ± SEM, $n = 3$). $^{*}P < 0.001$ versus CCL28-untreated control cells; $^{\#}P < 0.005$ and $^{\#\#}P < 0.001$ versus CCL28-only-treated cells by 1-way ANOVA with multiple-comparisons test. (**C**) Interaction between RARα and HDACs or DNMT in OSCC cells treated with CCL28 (20 pg/mL). Immune complexes were obtained using a Pierce Co-IP kit. (**A** and **C**) Representative Western blot images. (**D**) Acetylated histone H3 levels and HDAC1 interaction at the *RARB* promoter region of OSCC cells treated with CCL28 (20 pg/mL). Histone modification (H3K9ac) and HDAC1 binding were analyzed by ChIP-qPCR. Data are presented as the percentage of the total chromatin input (% input), and graphs are representative.

did not affect overall survival (Figure 8C). When CCL28, CCR3, CCR10, or RARβ expression was also categorized as low or high according to the median value of histoscore, high CCL28, CCR10, or RARβ expression was associated with a prolonged overall survival (Supplemental Figure 7). These results indicate that the possibility of bone invasion is higher in patients with OSCC with lower levels of CCL28, CCR10, or RARβ, leading to a poor prognosis.

Discussion

Patients with OSCC who have similar T stage tumors based on tumor size can have substantially different prognoses based on the presence of bone invasion. Patients with medullary invasion of the mandible suffer from distant metastases and locoregional recurrence (4, 40). Bone invasion in patients with OSCC is well recognized to predict poor prognosis, but the markers for the early

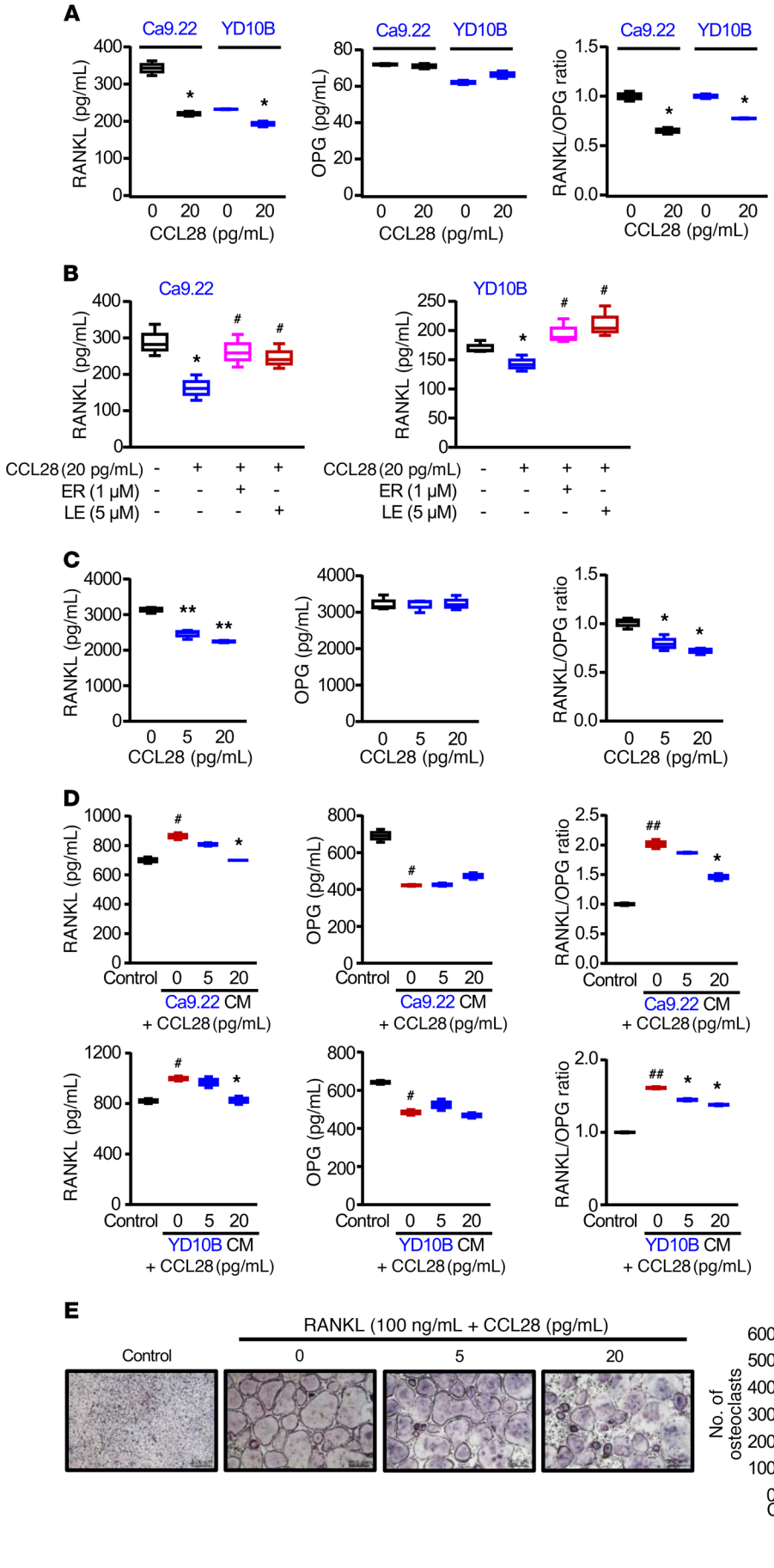

Figure 5. CCL28 treatment reduces the RANKL/OPG ratio in OSCC cells and osteoblasts and RANKL-induced differentiation of osteoclast precursors. (**A**) RANKL and OPG levels secreted by CCL28-treated OSCC cells into the culture media, and the RANKL/OPG ratio (mean ± SEM, $n = 3$). $^{*}P < 0.05$ vs. CCL28-untreated cells by 2-tailed Student's t test. (**B**) RANKL levels secreted by OSCC cells treated with the selective RARα antagonist ER50891 or the RARβ antagonist LE135 in the presence of CCL28 (mean ± SEM, $n = 3$). $^{*}P < 0.05$ versus CCL28-untreated cells; $^{\#}P < 0.05$ versus CCL28-only-treated cells by 1-way ANOVA with multiple comparisons test. (**C**) RANKL and OPG levels secreted by CCL28-treated osteoblasts into the culture media, and the RANKL/OPG ratio (mean ± SEM, $n = 3$). $^{*}P < 0.05$ and $^{**}P < 0.01$ versus CCL28-untreated cells by 1-way ANOVA with multiple comparisons test. (**D**) Secreted levels of RANKL and OPG by CCL28-treated osteoblasts in the presence of conditioned media (CM) from OSCC cell lines, and the RANKL/OPG ratio (mean ± SEM, $n = 3$). $^{\#}P < 0.05$ and $^{\#\#}P < 0.01$ versus control cells without CM; $^{*}P < 0.05$ versus CM-only-treated cells by 1-way ANOVA with multiple-comparisons test. (**E**) Osteoclast formation in CCL28-treated BMMs in the presence of RANKL (mean ± SEM, $n = 3$). Representative images at ×100 original magnification. $^{*}P < 0.05$ versus RANKL-only-treated cells by 1-way ANOVA with multiple comparisons test.

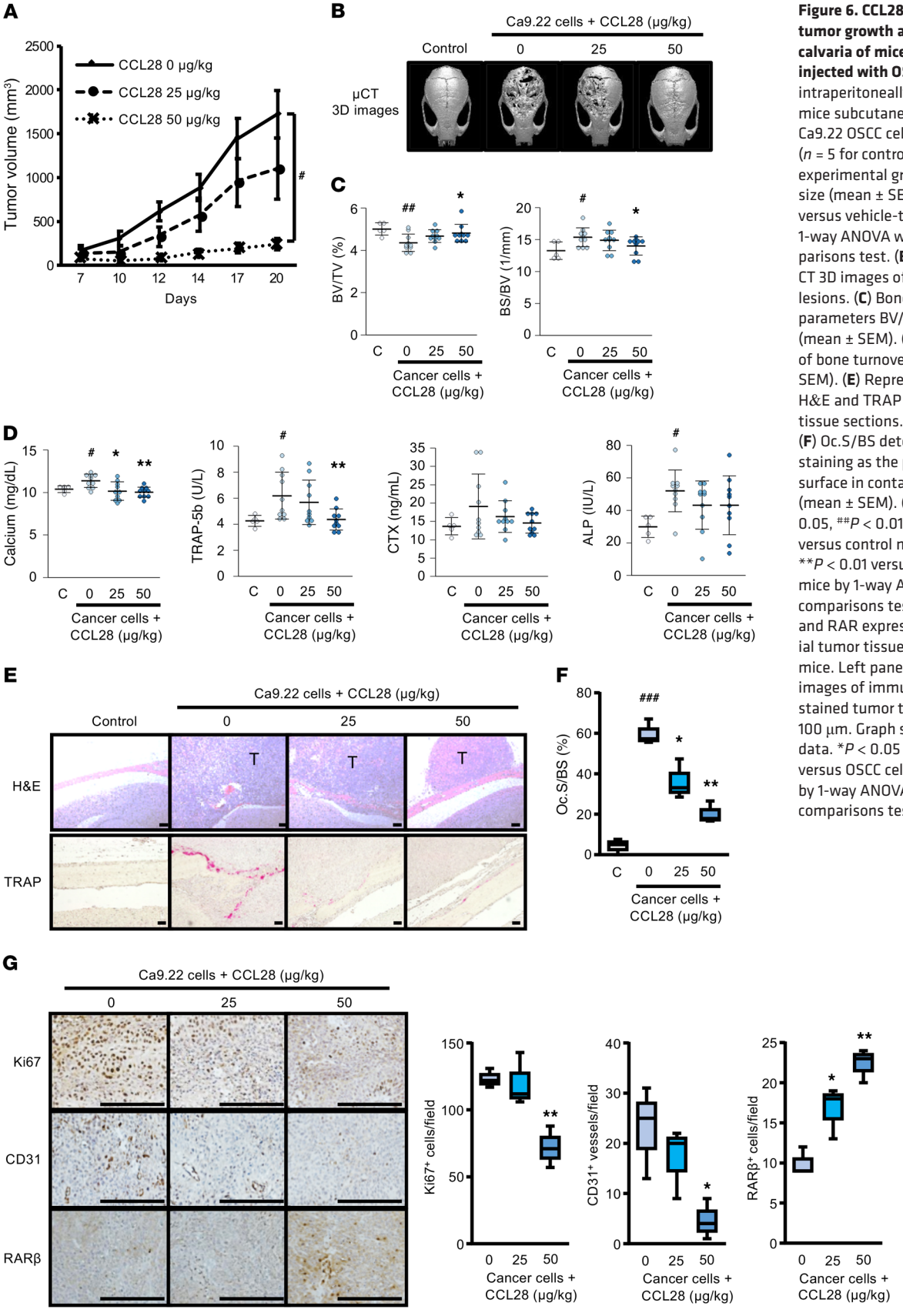

Figure 6. CCL28 treatment inhibits tumor growth and osteolysis in the calvaria of mice subcutaneously injected with OSCC cells. CCL28 was intraperitoneally administered to mice subcutaneously injected with Ca9.22 OSCC cells in the calvaria (n = 5 for control and n = 10 for experimental groups). (**A**) Tumor size (mean ± SEM). $^{\#}P < 0.001$ versus vehicle-treated mice by 1-way ANOVA with multiple comparisons test. (**B**) Representative CT 3D images of calvarial osteolytic lesions. (**C**) Bone morphometric parameters BV/TV and BS/TV (mean ± SEM). (**D**) Serum levels of bone turnover markers (mean ± SEM). (**E**) Representative images of H&E and TRAP staining in calvarial tissue sections. Scale bars: 100 μm. (**F**) Oc.S/BS determined from TRAP staining as the percentage of bone surface in contact with osteoclasts (mean ± SEM). (**C**, **D**, and **F**) $^{\#}P < 0.05$, $^{\#\#}P < 0.01$, and $^{\#\#\#}P < 0.005$ versus control mice; $^{*}P < 0.05$ and $^{**}P < 0.01$ versus OSCC cell–injected mice by 1-way ANOVA with multiple comparisons test. (**G**) Ki67, CD31, and RAR expression levels in calvarial tumor tissues of OSCC-injected mice. Left panel: Representative images of immunohistochemically stained tumor tissues. Scale bars: 100 μm. Graph shows quantified data. $^{*}P < 0.05$ and $^{**}P < 0.01$ versus OSCC cell–injected mice by 1-way ANOVA with multiple-comparisons test.

diagnosis and prognostic prediction of OSCC bone invasion remain largely unknown. We previously reported the oncogenic function of RUNX3 in OSCC bone invasion, although its role in OSCC is still controversial (27, 41). Here, we delineate the epigenetic mechanism by which CCL28 inhibits bone invasion of OSCC cells and subsequent osteolysis and its potential as a predictive and prognostic indicator for OSCC bone invasion.

OSCC bone invasion and osteolysis are triggered by factors expressed or secreted by cancer cells and are amplified through interactions among cancer cells, osteoblasts, and osteoclasts (5, 7). For OSCC, a poorer prognosis was reported in patients with more than 50% of podoplanin-positive tumor cells than in other patients (42). Insulin-like growth factor-II mRNA–binding protein-3 or podoplanin expression was correlated with T stage, lymph node metastasis, and overall survival in patients with OSCC; additionally, the combined expression of these proteins was associated with bone invasion (43). Gingival SCC patients with strong expression of VEGF displayed more aggressive bone invasion (44). Higher serum levels of CXCL9, cytokeratin 19 fragment, and C-reactive proteins have also been detected in patients with OSCC with bone invasion (24, 45). OSCC-derived chemokines have been reported to promote bone invasion mainly by increasing the invasive capacity of cancer cells (9, 25, 46). In this study, we found that CCL28 was downregulated by RUNX3 in Ca9.22 and YD10B OSCC cells. CCL28 inhibited the invasion of 2 OSCC cell lines expressing RUNX3, although indirect contributions of phenotypes, such as cell cycle arrest or apoptosis-unrelated forms of cell death, to the anti-invasive effect of CCL28 could not be fully excluded. Furthermore, CCL28 gene expression was downregulated in tumor tissues of HNSCC patients and correlated with overall survival, as shown by TCGA HNSCC data set analysis. These findings suggest that RUNX3-expressing OSCC cells, but not all OSCC cells, are responsive to the anti-invasive activity of CCL28. CCL28 gene expression levels may be associated with the progression of HNSCC, including oral cancer.

CCL28 is constitutively produced by epithelial cells of various mucosal tissues and contributes to the regulation of host mucosal defense under physiological conditions and during infection or inflammation. The role of CCL28 in human cancer is controversial. CCL28 protein levels in patients with colon and breast tumors and CCL28 mRNA and protein levels in pleomorphic adenomas and adenolymphoma of human salivary glands were significantly lower than in paired normal tissues (47–49). A reduction in CCL28 production in colon tumors was suggested to promote tumor progression by impairing the migration of IgA-secreting cells, which mediate tumor-specific cytotoxicity through NK cells or PMN phagocytes, into tumors (50). The induction of CCL28 in tumor cells was suggested to enhance cytotoxicity by attracting CCR10-expressing activated NK cells toward tumor sites (51). On the other hand, upregulated CCL28 under hypoxic conditions has been shown to promote angiogenesis via endothelial CCR3 in lung adenocarcinoma and recruitment of Tregs and tumor growth in liver and ovarian cancer (52–54). CCL28 overexpression stimulated breast cancer growth and metastasis by upregulating the antiapoptotic protein Bcl-2 and suppressing β-catenin (55) and promoted esophageal SCC cell migration (56). A recent study reported that CCL28 was a favorable prognostic factor for the luminal-like subtype of breast cancer but a poor prognostic indicator for the triple-negative subtype (57). Thus, the silencing or upregulation of CCL28 may be influenced by epithelial tumors of different origins. The role of CCL28 expression and its receptors and the underlying molecular mechanisms in epithelial tumors remain unknown. In this study, the invasion of RUNX3-expressing Ca9.22 and YD10B OSCC cells was inhibited by CCL28 treatment and CCL28 overexpression but improved by the knockdown of CCL28. Furthermore, CCL28 treatment inhibited EMT in CCL28-responsive OSCC cells by upregulating E-cadherin expression levels and reducing the expression levels of EMT-related transcription factors and nuclear β-catenin levels. Knockdown of CCL28 receptors, CCR3 and CCR10, did not affect cell invasion, but the anti-invasive effect of CCL28 was blocked in CCR10-knockdown cells. Therefore, the downregulation of CCL28 contributes to the acquisition of invasive ability in CCL28-responsive OSCC cells. The invasion of these OSCC cells can be blocked via CCR10 by elevation of CCL28 levels in the tumor microenvironment.

We further found that CCL28 signaling via CCR10 inhibited the invasiveness of CCL28-responsive OSCC cells by the reduced interaction between RARα and HDAC1 on RAREs and the subsequent induction of RARβ2. Moreover, compared with those in normal cells, reduced RARβ mRNA and/or protein levels or loss of RARβ expression have been detected in cells of various cancer types, including breast, head and neck, and lung cancer (58, 59). Overexpression of RARβ induced growth arrest and apoptosis in HSC4 and HO-1-N-1 oral cancer cell lines that have very low RARβ expression and resistance to RA (60), and downregulation of RARβ blocked the growth-inhibitory effect of RA in HNSCC cells (61). In addition, induction of RARβ increased retinoid sensitivity and suppressed EMT in cancer cells (62–64). RARβ expression has been reported to be activated by a rapid demethylation of its gene promoter or the removal of HDAC1 from the RARβ gene (65, 66). Our data demonstrate that the downregulation of CCL28 in OSCC cells reduces RARβ expression, improving the invasive ability of OSCC cells. The binding of CCL28 to CCR10 may enhance RARβ expression by blocking the recruitment of HDAC1 to the transcriptional corepressor complex interacting with RARs.

The development of OSCC cell–mediated osteolytic lesions is finally caused by osteoclasts. RANKL signaling via RANK in osteoclast precursors regulates osteoclastogenesis. OSCC cell lines were found to secrete RANKL both directly and via osteoblastic/stromal cells (67). OSCC-derived chemokines, including MCP-1, CXCL8, and CXCL13, stimulated RANKL expression and RANKL-induced osteoclastogenesis (23, 25, 68). In contrast with these chemokines, CCL28 reduced the production of RANKL, and this reduced RANKL production appeared to be associated with CCL28-induced RARβ expression in CCL28-responsive OSCC cells. Moreover, CCL28 inhibited the secreted levels of RANKL in osteoblastic cells exposed or not exposed to OSCC cell–derived conditioned media and blocked the RANKL-induced formation of active osteoclasts. Thus, CCL28 can prevent osteoclast-mediated bone loss by blocking RANKL production in OSCC cells and osteoblastic cells and RANKL-induced differentiation of osteoclast precursors.

The inhibitory effect of CCL28 on OSCC cell–mediated osteolysis was confirmed in 2 murine models for cancer cell

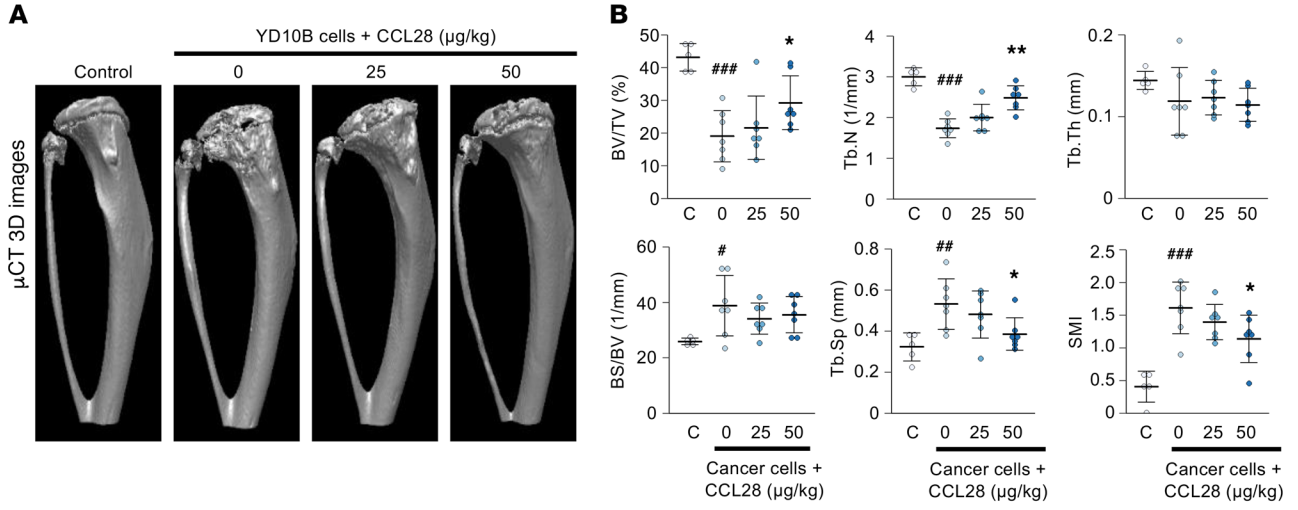
A
YD10B cells + CCL28 (μg/kg)
Control
0
25
50
μCT 3D images
B
BV/TV (%)
Tb.N (1/mm)
Tb.Th (mm)
BS/BV (1/mm)
Tb.Sp (mm)
SMI
C 0 25 50
Cancer cells + CCL28 (μg/kg)

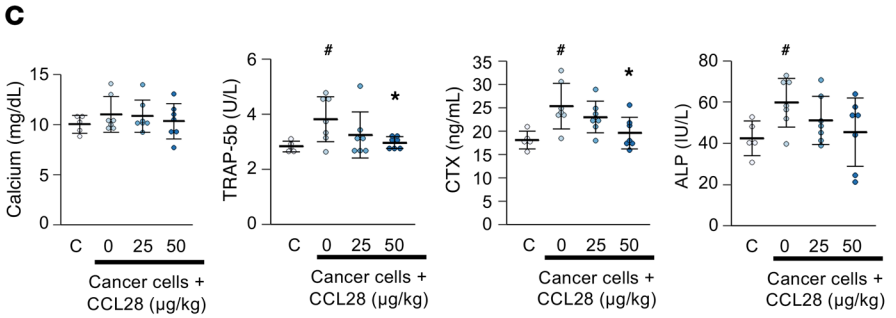
C
Calcium (mg/dL)
TRAP-5b (U/L)
CTX (ng/mL)
ALP (IU/L)
C 0 25 50
Cancer cells + CCL28 (μg/kg)

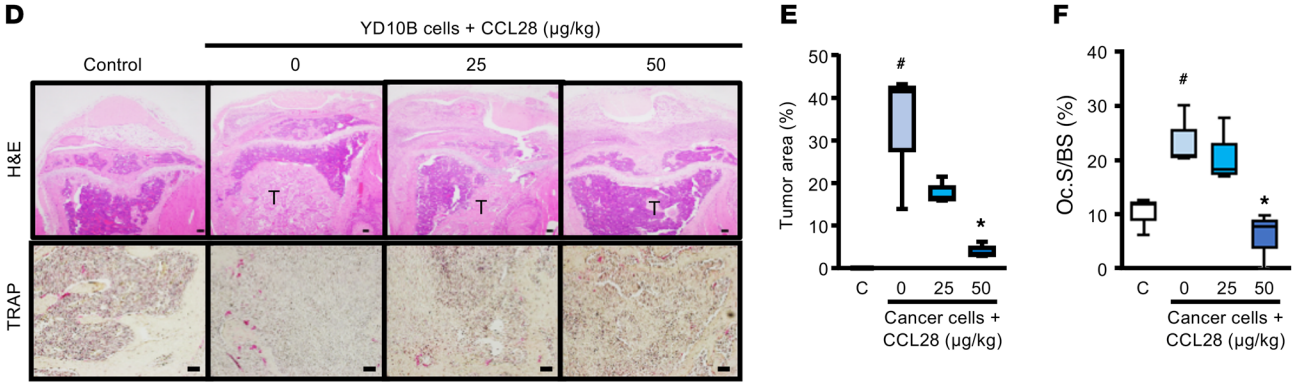
D
YD10B cells + CCL28 (μg/kg)
Control
0
25
50
H&E
TRAP
T
E
Tumor area (%)
F
Oc.S/BS (%)
C 0 25 50
Cancer cells + CCL28 (μg/kg)

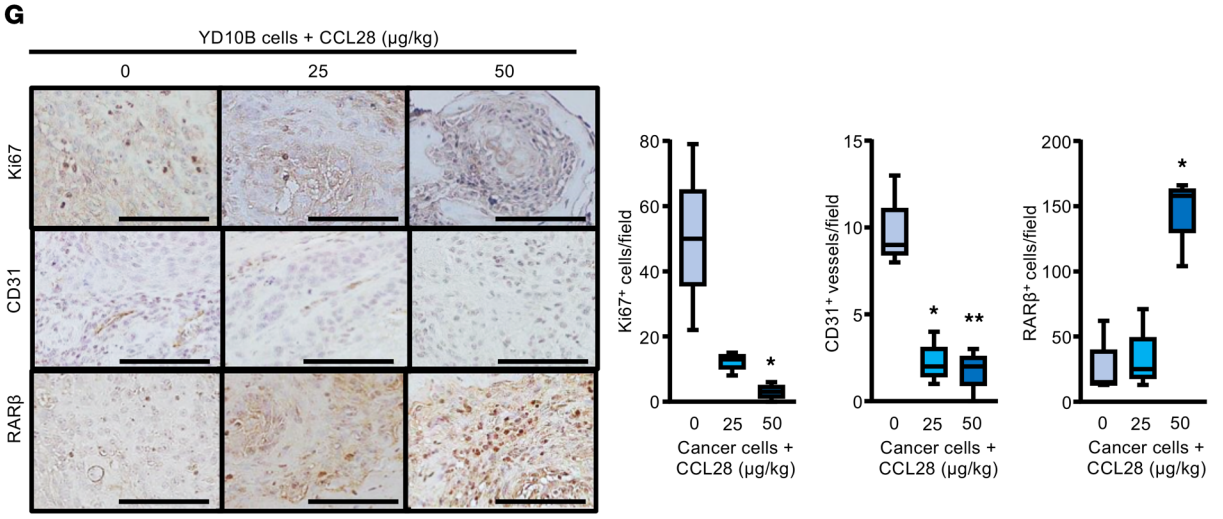
G
YD10B cells + CCL28 (μg/kg)
0
25
50
Ki67
CD31
RARβ
Ki67+ cells/field
CD31+ vessels/field
RARβ+ cells/field
Cancer cells + CCL28 (μg/kg)

Figure 7. CCL28 treatment inhibits tumor growth and osteolysis in mice intratibially injected with OSCC cells. CCL28 was intraperitoneally administered to mice injected with YD10B OSCC cells into the bone marrow of the right tibia (n = 5 for control and n = 7 for experimental groups). (**A**) Representative CT 3D images of osteolytic lesions in the tibia. (**B**) Bone morphometric parameters (mean ± SEM). (**C**) Serum levels of bone turnover markers (mean ± SEM). (**D**) Representative images of H&E and TRAP staining in tibial tissue sections. Scale bars: 100 μm. (**E**) Tumor area determined from H&E staining as the percentage of the total tumor area per tissue area. (**F**) Oc.S/BS determined from TRAP staining as the percentage of bone surface in contact with osteoclasts (mean ± SEM). (**B**, **C**, **E**, and **F**) $^{\#}P < 0.05$, $^{\#\#}P < 0.01$, and $^{\#\#\#}P < 0.005$ versus control mice; $^{*}P < 0.05$ and $^{**}P < 0.01$ versus OSCC cell–injected mice by 1-way ANOVA with multiple comparisons test. (**G**) Ki67, CD31, and RARβ expression levels in tibial tumor tissues of OSCC-injected mice. Left panel: Representative images of immunohistochemically stained tumor tissues. Scale bars: 100 μm. Right panel: Ki67-positive cells, CD31-positive vessels, and RARβ-positive cells were counted in tumor tissues. $^{*}P < 0.05$ and $^{**}P < 0.01$ versus OSCC cell–injected mice by 1-way ANOVA with multiple comparisons test.

bone invasion. Intraperitoneally administered CCL28 prevented osteolysis in athymic nude mice inoculated with OSCC cells. The anti-osteoclastogenic activity of CCL28 was supported by the reduced number of TRAP-positive osteoclasts detected at the interface between tumor and bone tissues. Tumor growth was also inhibited by CCL28 treatment, and the in vivo inhibitory activity of CCL28 on tumor growth may be due to a decrease in the release of bone matrix–derived growth factors by osteoclast-mediated bone resorption rather than the direct inhibition of OSCC cell viability. Increased RARβ expression was detected in the tumor tissues of CCL28-treated mice. Furthermore, we confirmed that CCL28 overexpression in OSCC cells can also reduce tumor growth and osteolysis. These findings support the in vitro results demonstrating that CCL28 inhibits OSCC bone invasion by upregulating RARβ.

In patients with OSCC, bone invasion was detected at a higher frequency than perineural and vascular invasion. This higher frequency of bone invasion may be associated with the anatomical closeness of the lesions to bone. Downregulated CCL28, CCR10, or RARβ expression was closely related to bone invasion. Therefore, CCL28, CCR10, and RARβ expression levels are useful markers for the prediction and prognosis of OSCC bone invasion. Furthermore, CCL28 treatment or CCL28 upregulation in OSCC cells may be a novel strategy for inhibiting and treating OSCC cell invasion and osteolysis. Further studies are needed to determine whether CCL28 can also prevent bone invasion and osteolysis of bone-tropic cancer cells, including breast, prostate, and lung cancer cells.

Methods

Reagents. DMEM, α-MEM, DMEM/nutrient mixture F-12 (DMEM/F-12) without phenol red, PBS, FBS, 0.25% trypsin-EDTA, Geneticin (G418), and 1% antibiotic-antimycotic mixture were purchased from Gibco BRL. Recombinant human CCL28 and TGF-β were obtained from PeproTech. MTT, Histopaque-1083, and puromycin were purchased from Sigma-Aldrich. Carboxyfluorescein diacetate succinimidyl ester (CFDA-SE), blasticidin S, HRP–goat anti-rabbit IgG (H+L), and Lipofectamine RNAiMAX reagent were obtained from Invitrogen. Matrigel was purchased from BD Biosciences. The selective RARβ antagonist LE135, the inverse pan-RAR agonist BMS493, and the selective RARα antagonist ER50891 were purchased from Tocris. Recombinant mouse soluble RANKL and macrophage CSF (M-CSF) were purchased from R&D Systems. All reagents used in this study were of analytical grade.

Antibodies. Anti-RUNX3 (ab40278), anti-CCL28 (ab196567), anti-CCR3 (ab32512), anti-CCR10 (ab196567), anti-RARβ (ab124701), anti-CD31 (ab28364), anti-Ki67 (ab15580), and anti-rabbit secondary antibodies (ab97051) were purchased from Abcam. Anti-GAPDH (sc32233), anti–E-cadherin (sc8426), anti–β-catenin (sc1496R), anti–lamin A/C (sc7293), anti-CCR10 (sc365957), anti-RARα (sc551), anti-RARβ2 (sc514585), anti-RANKL (sc9073), and anti-OPG (sc71747) antibodies and control IgG (sc2027) were purchased from Santa Cruz Biotechnology. Anti-Slug (9585S), anti-Twist1 (46702S), anti-Snail (3879S), anti-HDAC1 (34589S), anti-HDAC2 (57156S), anti-HDAC3 (85057S), anti–acetyl-histone H3 (9649S), anti-DNMT1 (5032S), anti–caspase-3 (9662S), anti-PARP (9542S), and anti-mouse (7076S) secondary antibodies were purchased from Cell Signaling Technology.

Animals. Five-week-old male BALB/c nude mice (19 ± 1 g) were purchased from Orient Bio, and 4-week-old male ICR mice (21 ± 2 g) were obtained from NARA Biotech. The mice were given free access to commercial rodent chow and tap water and housed under specific pathogen–free conditions with a relative humidity of 50% ± 5% and a 12-hour light/12-hour dark cycle at 22°C ± 2°C.

Cell lines and cell culture. Ca9.22, HSC2, and HSC3 OSCC cells were purchased from the Japanese Collection of Research Bioresources Cell Bank (Shinjuku, Japan). YD10B OSCC cells were obtained from the Department of Oral Pathology, College of Dentistry, Yonsei University (Seoul, Korea) (69). RUNX3-knockdown Ca9.22 and YD10B cells were established in our previous study (27). These cells were grown in DMEM supplemented with 10% FBS and 1% antibiotic-antimycotic mixture at 37°C in a humidified atmosphere with 5% CO_2. The hFOB1.19 osteoblastic cells were purchased from American Type Culture Collection and maintained at 34°C in DMEM/F-12 without phenol red but containing 10% FBS, 0.3 mg/mL G418, and a 1% antibiotic-antimycotic mixture. BMMs were isolated from the tibiae of 4-week-old ICR male mice using Histopaque-1083 density gradient centrifugation. BMMs were cultured in α-MEM containing 10% FBS, 30 ng/mL M-CSF, and 1% antibiotic-antimycotic mixture at 37°C in a humidified atmosphere with 5% CO_2.

PCR array of chemokines and their receptors. Total RNA was extracted from RUNX3-expressing or RUNX3-knockdown Ca9.22 cells using an RNeasy Mini Kit (Qiagen). cDNA was synthesized from extracted RNA using an RT^2 First Strand Kit (SABiosciences). The cDNA was mixed with RT^2 SYBR Green/ROX qPCR Master Mix (SABiosciences), and the mixture was added into a 96-well RT^2 PCR Array (SABiosciences) that includes primer pairs for 84 human genes encoding chemokines and their receptors. Quantitative real-time PCR analysis was conducted using the 7300 Real-Time PCR System (Applied Biosystems) according to the manufacturer's instructions. Changes in gene expression by RUNX3 knockdown were determined on the basis of cycle thresholds using Web-based RT^2 Profiler PCR Array Data Analysis Software (SABiosciences). Changes in gene expression by RUNX3 knockdown were expressed as fold changes using the comparative ΔΔCt method.

Knockdown of CCL28, CCR3, or CCL10. To establish OSCC cells with stable knockdown of CCL28, CCR3, or CCR10, the cells were infected with shRNA-containing lentiviral particles (Sigma-Aldrich).

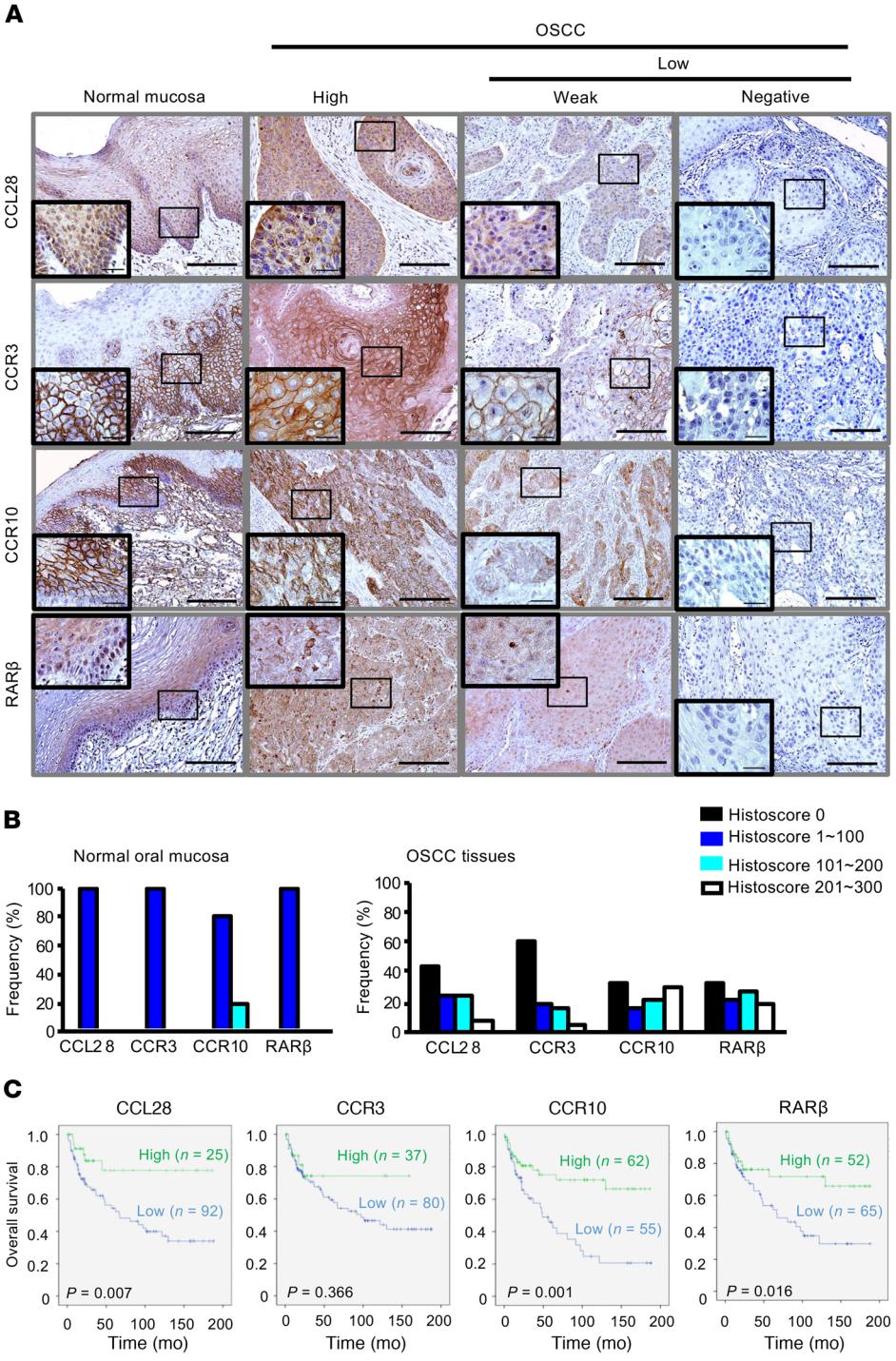

Figure 8. Expression levels of CCL28, CCR10, or RARβ are closely associated with overall survival in 117 patients with OSCC. (**A**) Representative images of IHC staining of CCL28, CCR3, CCR10, and RARβ in normal oral mucosa and OSCC tissues. Scale bars: 100 μm. Magnified images of the boxed area are shown in the insets. Scale bars: 20 μm. (**B**) Frequency of histoscores in normal oral mucosa and OSCC tissues. (**C**) Kaplan-Meier survival curve of patients with OSCC stratified based on CCL28, CCR3, CCR10, or RARβ expression by the log-rank test.

One negative control shRNA (SHC002V) and 3 different shRNAs (SHCLNV-NM_020279, SHCLNV-NM_016602, and SHCLNV-NM_001837) were used for each gene. OSCC cells were seeded in 60-mm dishes, and the cells were incubated with viral supernatants in the presence of 10 μg/mL Polybrene (Santa Cruz Biotechnology) for 24 hours. After the viral supernatants were removed, the infected cells were cultured in fresh medium containing 10% FBS for 2 days and then incubated in medium containing 10% FBS and 10 μg/mL puromycin for an additional 2 weeks. In addition, Ca9.22 and YD10B cells (3×10^5 cells per well) were transfected with negative control siRNAs, CCR3-targeting siRNAs, or CCR10-targeting siRNAs (Santa Cruz Biotechnology) using Lipofectamine RNAiMAX reagent (Invitrogen) according to the manufacturer's instructions.

Overexpression of RUNX3 or CCL28. Stable RUNX3- or CCL28-overexpressing OSCC cells were established with the lentiviral gene expression system (Lenti-CMV-GFP-2A-Puro, LVP690, LVP802266, and LVP110389) from Applied Biological Materials according to the manufacturer's instructions.

MTT assay. OSCC cells (2×10^3 cells per well) were seeded in 96-well plates. OSCC cells were treated with CCL28 at the indicated concentrations for 24 and 72 hours. The cells were incubated with 20 μL of MTT (5 mg/mL) in PBS at 37°C for 4 hours. The medium was removed, and the cells were lysed with 200 μL of DMSO for 30 minutes at 37°C. Absorbance was determined at 570 nm using a microplate reader (Bio-Rad Laboratories).

Transwell invasion assay. The invasiveness of OSCC cells was determined using a 6.5-mm Transwell chamber with an 8.0-μm-pore polycarbonate membrane (Corning Costar). The lower and upper surfaces of the membrane were precoated with 1 mg/mL gelatin and Matrigel (BD Biosciences), respectively. OSCC cells (5×10^4 cells/0.1 mL) were seeded into the upper chamber with 5% FBS-DMEM and indicated concentrations of CCL28 in the absence or presence of TGF-β (10 ng/mL), LE135, BMS493, or ER50891. The lower chamber was filled with 0.6 mL of medium containing 10% FBS and the indicated concentration of CCL28. Twenty-four hours later, the number of invaded cells was counted under a microscope as previously described (70).

Chick CAM invasion assay. OSCC cells were labeled with 10 μM CFDA-SE in prewarmed PBS at 37°C for 15 minutes as previously described (71). Fertilized chicken eggs were purchased from a local distributor (Seoul, Korea) and kept in a humidified incubator at

Table 1. Relationships between clinicopathologic characteristics and the expression of CCL28, its receptors, or RARβ in 117 patients with OSCC

		CCL28 histoscore			CCR3 histoscore			CCR10 histoscore			RARβ histoscore		
	All *n* = 117 (%)	Low (0–100) *n* = 92 (%)	High (101–300) *n* = 25 (%)	*P*	Low (0–100) *n* = 80 (%)	High (101–300) *n* = 37 (%)	*P*	Low (0–100) *n* = 55 (%)	High (101–300) *n* = 62 (%)	*P*	Low (0–100) *n* = 65 (%)	High (101–300) *n* = 52 (%)	*P*
Age													
<62	58 (49.6)	34 (58.6)	24 (41.4)		42 (72.4)	16 (27.6)		24 (41.4)	34 (58.6)		27 (46.6)	31 (53.4)	
≥62	59 (50.4)	46 (78.0)	13 (22.0)	0.024	50 (84.7)	9 (15.3)	0.104	31 (52.5)	28 (47.5)	0.226	38 (64.4)	21 (35.6)	0.052
Sex													
Male	78 (66.7)	54 (69.2)	24 (30.8)		61 (78.2)	17 (21.8)		36 (46.2)	42 (53.8)		46 (59.0)	32 (41.0)	
Female	39 (33.3)	26 (66.7)	13 (33.3)	0.779	31 (79.5)	8 (20.5)	0.873	19 (48.7)	20 (51.3)	1	19 (48.7)	20 (51.3)	0.293
Lesion site													
Tongue	23 (19.7)	9 (39.1)	14 (60.9)		16 (69.6)	7 (30.4)		7 (30.4)	16 (69.6)		8 (34.8)	15 (65.2)	
Floor of mouth	6 (5.1)	5 (83.3)	1 (16.7)		4 (66.7)	2 (33.3)		3 (50.0)	3 (50.0)		3 (50.0)	3 (50.0)	
Retromolar trigone	15 (12.8)	11 (73.3)	4 (26.7)		13 (86.7)	2 (13.3)		6 (40.0)	9 (60.0)		8 (53.3)	7 (46.7)	
Gingiva	62 (53.0)	48 (77.4)	14 (22.6)		52 (83.9)	10 (16.1)		33 (53.2)	29 (46.8)		40 (64.5)	22 (35.5)	
Cheek	11 (9.4)	7 (63.6)	4 (36.4)	0.015	7 (63.6)	4 (36.4)	0.32	6 (54.5)	5 (45.5)	0.397	6 (54.5)	5 (45.5)	0.189
T stage													
T1–2	41 (36.0)	25 (61.0)	16 (39.0)		29 (70.7)	12 (29.3)		17 (41.5)	24 (58.5)		19 (46.3)	22 (53.7)	
T3–4	73 (64.0)	54 (74.0)	19 (26.0)	0.149	61 (83.6)	12 (16.4)	0.107	38 (52.1)	35 (47.9)	0.277	45 (61.6)	28 (38.4)	0.114
N stage													
N0	67 (57.8)	44 (65.7)	23 (34.3)		52 (77.6)	15 (22.4)		28 (41.8)	39 (58.2)		36 (53.7)	31 (46.3)	
N1–3	49 (42.2)	36 (73.5)	13 (31.0)	0.37	40 (81.6)	9 (18.4)	0.597	27 (55.1)	22 (44.9)	0.156	29 (59.2)	20 (40.8)	0.559
Differentiation													
Well	28 (23.9)	18 (64.3)	10 (35.7)		21 (75.0)	7 (25.0)		11 (39.3)	17 (60.7)		10 (35.7)	18 (64.3)	
Moderate	70 (59.8)	51 (72.9)	19 (27.1)		56 (80.0)	14 (20.0)		33 (47.1)	37 (52.9)		43 (61.4)	27 (38.6)	
Poor	19 (16.2)	11 (57.9)	8 (42.1)	0.4	15 (78.9)	4 (21.1)	0.861	11 (57.9)	8 (42.1)	0.455	12 (63.2)	7 (36.8)	0.053
Perineural invasion													
No	100 (85.5)	65 (65.0)	35 (35.0)		77 (77.0)	23 (23.0)		43 (43.0)	57 (57.0)		51 (51.0)	49 (49.0)	
Yes	17 (14.5)	15 (88.2)	2 (11.8)	0.057	15 (88.2)	2 (11.8)	0.296	12 (70.6)	5 (29.4)	0.035	14 (82.4)	3 (17.6)	0.016
Vascular invasion													
No	107 (91.5)	72 (67.3)	35 (32.7)		86 (80.4)	21 (19.6)		47 (43.9)	60 (56.1)		58 (54.2)	49 (45.8)	
Yes	10 (8.5)	8 (80.0)	2 (20.0)	0.408	6 (78.6)	4 (40.0)	0.133	8 (80.0)	2 (20.0)	0.029	7 (70.0)	3 (30.0)	0.336
Bone invasion													
No	50 (42.7)	26 (52.0)	24 (48.0)		35 (70.0)	15 (30.0)		16 (32.0)	34 (68.0)		21 (42.0)	29 (58.0)	
Yes	67 (57.3)	54 (80.6)	13 (19.4)	0.001	57 (85.1)	10 (14.9)	0.049	39 (58.2)	28 (41.8)	0.005	44 (65.7)	23 (34.3)	0.011

37°C for 3 days. Three milliliters of egg albumin was removed with a syringe, and a small window was made using sterile scissors and forceps. The window was resealed with adhesive tape, and the eggs were incubated until 11 days of chick embryo development. On day 11, CFDA-SE–labeled OSCC cells were suspended in DMEM/Matrigel (4:1) mixture. The suspended CFDA-SE–labeled OSCC cells (1×10^6 cells per egg) were treated with CCL28 (50 pg/mL) and/or TGF-β (10 ng/mL) and loaded onto the CAMs of fertilized eggs (n = 3). The resealed eggs were further incubated for 3 days. On day 14, the CAMs were harvested and fixed with neutralized formalin for 24 hours. Images of CAM sections were obtained using a Zeiss LSM 700 confocal microscope (Zeiss Laboratories) and analyzed using ImageJ software (NIH). Cell invasion was determined by measurement of the mean fluorescence of cells that had invaded into the mesoderm layer (below the CAM surface).

Immunofluorescence staining and confocal imaging. OSCC cells (5×10^3 cells per well) were seeded in a chamber slide and incubated in complete medium for 24 hours. After treatment with CCL28 at the indicated concentrations in the absence or presence of TGF-β, ER50891, or LE135 for 24 hours, the cells were fixed with 4% paraformaldehyde and permeabilized with Triton X-100–containing buffer. The cells were blocked with 2% goat serum in PBS and then incubated with primary antibodies at 1:200 dilutions overnight at 4°C. After washing, the cells were incubated with Alexa Fluor 488 goat anti-mouse IgG and Alexa Fluor 594 goat anti-rabbit IgG (Invitrogen) for 1 hour at room temperature. The slides were mounted in Vectashield mounting medium with DAPI (Vector Laboratories). Images were collected using a Zeiss LSM 700 confocal microscope.

Western blot analysis. OSCC cells (1×10^6 cells per 100-mm dish) were treated with CCL28 at the indicated concentrations in the absence or presence of TGF-β, ER50891, or LE135 for 24 hours. Cell lysates were prepared using RIPA buffer containing a protease inhibitor cocktail (Cell Signaling Technology). The lysates were centrifuged at 22,000 *g* for 15 minutes at 4°C. Nuclear and cytosolic fractions were obtained from OSCC cell lysates using a nuclear/cytosol fractionation kit (BioVision) according to the manufacturer's instructions.

The protein concentration of samples was determined using a BCA kit (Pierce). Protein (20 μg) was loaded onto an SDS-polyacrylamide gel and electrophoresed, and the protein in the gels was transferred to a PVDF membrane (Millipore). The membrane was blocked with 5% skim milk in Tris-buffered saline (10 mM Tris, pH 8.0, and 150 mM NaCl) with 0.1% Tween-20 (TBS-T) and then incubated with primary antibodies (1:1000) in TBS-T containing 3% BSA. The membrane was further incubated with HRP-conjugated secondary antibodies in TBS-T containing 3% skim milk for 1 hour at room temperature. The targeted proteins were visualized with Amersham ECL Western Blotting Detection Reagents (GE Healthcare).

TCGA data mining. The TCGA HNSCC data set was generated by the TCGA Research Network. TCGA HNSCC data were obtained from the UCSC Cancer Genome Browser in August 2015 to analyze CCL28, CCR3, and CCR10 mRNA expression in head and neck cancer tissues (n = 519) and normal adjacent tissues (n = 43) and to determine the correlation of overall survival and mRNA expression levels of CCL28 or its receptors (n = 505). Normalized RNA Sequencing by Expectation Maximization (RSEM) values were used to generate box plots of genes and assess the correlation of gene expression. The RA signature is determined by the sum of the expression values of genes that are known to be regulated by an agonist of the RAR as previously described (72).

Pathway reporter array. Pathway analysis was conducted using the Cignal Finder 45-Pathway Reporter Array (SABiosciences) according to the manufacturer's instructions. Twenty-four hours after cells were reversely transfected, the cells were treated with 20 pg/mL CCL28 and then incubated for another 24 hours. Luciferase activity was measured using the Dual-Luciferase Assay system (Promega) with a luminescence microplate reader (Varioskan Flash 3001, Thermo Fisher Scientific). Firefly luciferase was the experimental reporter, and *Renilla* luciferase was the normalizing reporter. The fold change in the activity of each signaling pathway was calculated from the normalized luciferase activities in treated versus untreated cells.

Co-IP. Co-IP assays were performed using the Pierce Co-IP Kit (Thermo Fisher Scientific). Briefly, OSCC cells (1×10^6 cells per 100-mm dish) were incubated in medium containing 10% FBS for 24 hours and treated with 20 pg/mL CCL28 for an additional 24 hours. The cells were lysed using 500 μL of lysis buffer, and 50 μL of whole lysate was removed for SDS-PAGE as the input control. The remaining cell lysate was incubated and immunoprecipitated with 20 μg of primary antibody against RARα and 25 μL of AminoLink Plus Coupling Gel (Thermo Fisher Scientific) at 4°C overnight. The immune complexes were washed 5 times and eluted using IgG elution buffer. The eluted immune complexes were boiled at 95°C in SDS–sample buffer for 5 minutes and detected by Western blotting.

ChIP. ChIP assays were performed using the Simple ChIP Enzymatic Chromatin IP Kit (Cell Signaling Technology, 9002), following the manufacturer's protocol. Anti-HDAC1 and anti–acetyl-histone H3 (K9) antibodies were used for chromatin precipitation, while anti–histone H3 and rabbit IgG antibodies served as positive and negative controls, respectively. All antibodies were diluted 1:50. Following DNA purification, the presence of selected DNA sequences was assessed by quantitative PCR (qPCR) using the following primers: *RARB*: forward, 5′-GTTCACCGAAAGTTCACTCGCA-3′, and reverse, 5′-CAAAGAATAGACCCTCCTGCCTCT-3′; *RPL30* (Cell Signaling Technology, 7014). As a loading control, the qPCR was performed directly on input DNA purified from chromatin before IP. Data are presented as the amount of DNA recovered relative to the input control.

Preparation of conditioned media. OSCC cells (1×10^5 cells per dish) were seeded in 100-mm culture dishes for 24 hours. The cells were cultured in fresh medium containing 10% FBS for 24 hours. The culture media were centrifuged at 500 *g* for 5 minutes. The supernatants were used as conditioned media for subsequent experiments.

ELISA. OSCC cells (2×10^3 cells per well) were cultured for 24 or 72 hours. In addition, OSCC cells were treated with CCL28 at the indicated concentrations in the absence or presence of ER50891 (1 μM) or LE135 (5 μM) for 24 hours. hFOB1.19 osteoblasts (5×10^3 cells per well) were treated with CCL28 at the indicated concentrations in the absence or presence of OSCC-conditioned medium for 24 hours. CCL28, RANKL, or OPG levels in cell culture media were measured with commercially available kits for CCL28 (BioLegend), RANKL (EIAab), or OPG (Boster) according to the manufacturer's instructions.

Osteoclast formation. BMMs (5×10^4 cells) were treated with CCL28 at the indicated concentrations or with 30% conditioned media from CCL28-overexpressing or CCL28-knockdown OSCC cells, together with M-CSF (30 ng/mL) and RANKL (100 ng/mL) for 5 days. The medium was replaced with fresh medium every 2 days. The cells were fixed with fixative solution for 30 seconds at room temperature, and enzyme histochemistry for TRAP was performed with a commercial kit (Sigma-Aldrich) according to the manufacturer's instructions. Multinuclear TRAP-positive cells (≥3 nuclei) were considered osteoclasts.

Murine calvarial and intratibial models of cancer-associated osteolysis. For the calvarial model, 6-week-old male BALB/c nude mice were randomly divided into groups. Ca9.22 cells (1×10^7 cells per 100 μL of HBSS) were subcutaneously inoculated over the calvaria of mice using a 1-mL syringe with a sterile 26-gauge needle, and the control mice were injected with HBSS alone. CCL28 at the indicated doses in PBS was intraperitoneally injected. In addition, CCL28-overexpressing Ca9.22 cells or Ca9.22 cells with empty vector were subcutaneously inoculated over the calvaria of mice. Tumor volumes at the calvaria were measured using a digital electric caliper and calculated according to the formula $(a \times b^2)/2$, where a is the longest diameter and b is the shortest diameter of the tumor. On day 21, blood, calvaria, and tumor were collected. For the intratibial model, 6-week-old male BALB/c nude mice were anesthetized using an intraperitoneal injection of a mixture of 30 mg/kg Zoletil (Virbac Laboratories) and 10 mg/kg Rompun (Bayer HealthCare Korea). YD10B cells (1×10^6 cells per 50 μL of HBSS) were injected into the bone marrow of the right tibia of mice through the femorotibial cartilage using a Hamilton syringe with a sterile 27-gauge needle. The control mice were injected with HBSS alone. CCL28 at the indicated doses was intraperitoneally injected. On day 28, the tibiae and blood were collected.

The effect of CCL28 on OSCC bone invasion was analyzed as previously described (26, 27). The collected calvaria and tibiae were analyzed scanned with a micro-CT (μCT) system (SkyScan 1076). 3D images were generated using NRecon software (SkyScan), and bone morphometric parameters, including BV/TV, BS/TV, BS/BV, trabecular thickness (Tb.Th), Tb.N, Tb.Sp, or SMI, were analyzed from μCT data using CTAn software (SkyScan). Serum levels of calcium were determined using the QuantiChrome Calcium assay kit (BioAssay Systems), and serum levels of TRAP-5b and CTX were measured using a

mouse TRAP assay kit (Immuno Diagnostic Systems) and a RatLaps enzyme immunoassay kit (Immuno Diagnostic Systems), respectively. H&E and TRAP staining was also performed on mouse calvarial or hind-limb sections. Tumor areas and osteoclast surface per bone surface (Oc.S/BS) were measured with IMT i-Solution software (version 7.3, IMT i-Solution). Tumor areas were calculated as the percentage of total tumor area per tissue area. Oc.S/BS values were determined as the percentage of bone surface in contact with osteoclasts. The expression levels of PCNA, CD31, and RARβ in tumor tissues were evaluated by IHC examination with a 1:100 dilution of each primary antibody against PCNA, CD31, and RAR.

Immunostaining of formalin-fixed, paraffin-embedded OSCC samples. One hundred seventeen formalin-fixed, paraffin-embedded OSCC tissues were analyzed by IHC staining using anti–rabbit CCL28, CCR3, CCR10, or RARβ antibody. Mouse IgG or rabbit IgG (Dako-Cytomation) was used as a negative control. The expression levels of CCL28, CCR3, CCR10, and RARβ were interpreted using a weighted histoscore method. Staining was scored by Yan Chen and Yan Peng, who were blinded to clinical data, and classified into 4 grades (range 0–3) according to the percentage of immunopositive cells and immunostaining intensity: 0 (negative), 1 (light brown), 2 (brown), or 3 (dark brown). The histoscore was then calculated as follows: final score = (0 × percentage of negative cells) + (1 × percentage of light brown cells) + (2 × percentage of brown cells) + (3 × percentage of dark brown cells). The samples were subsequently divided into 2 groups according to final histoscores: low expression (histoscores from 0 through 100) and high expression (histoscores from 101 through 300).

Statistics. The results are expressed as the mean ± SEM of 3 independent experiments. One representative experiment from multiple experiments is shown. Two-tailed Student's *t* test and 1-way ANOVA with multiple-comparisons test were used for comparisons between 2 groups and among more than 3 groups, respectively. The data retrieved from the TCGA website were reanalyzed to determine Pearson's correlation coefficients (*r*) between CCL28 mRNA expression and RARβ mRNA expression. Kaplan-Meier survival curves were compared using the log-rank test. The χ^2 test was used to evaluate the relation between CCL28, CCR3, CCR10, or RARβ expression and different clinicopathologic parameters of patients. All statistical analyses were performed using SPSS version 19.0 (SPSS Inc.). *P* less than 0.05 was considered statistically significant.

Study approval. All animal experiments were approved by the IACUC of the Department of Laboratory Animal Resources, Yonsei Biomedical Research Institute, Yonsei University College of Medicine (Approval number 2013-0100-1 and 2015-0355). Human OSCC tissues were obtained from patients at the Department of Oral and Maxillofacial Surgery, Dental Hospital, Yonsei University Medical Center, from 1995 to 2016, and the study was approved by the institutional review board at Yonsei University College of Dentistry (Approval number 2-2017-0004). All patients provided written informed consent prior to inclusion in the study.

Author contributions

WYC and JP conceived and designed the study. JP, SKL, and XZ performed experiments and data analysis. NYS, SHS, KRK, JHS, and KKP contributed to experimental design and data analysis. JP, KKP, and WYC contributed to manuscript writing. All authors revised and edited the manuscript.

Acknowledgments

We thank Chae-Eun Lee from the Oral Science Research Institute for providing technical assistance with μCT. This research was supported by a grant from the Korea Health Technology R&D Project through the Korea Health Industry Development Institute (KHIDI), funded by the Ministry of Health & Welfare, Republic of Korea (HI15C1901).

Address correspondence to: Won-Yoon Chung, Department of Oral Biology, Yonsei University College of Dentistry, Yonsei University, 50-1 Yonsei-ro, Seodaemun-gu, Seoul 03722, Korea. Phone: 82.2.2228.3057; Email: wychung@yuhs.ac.

1. Jimi E, Furuta H, Matsuo K, Tominaga K, Takahashi T, Nakanishi O. The cellular and molecular mechanisms of bone invasion by oral squamous cell carcinoma. *Oral Dis*. 2011;17(5):462–468.
2. Takes RP, et al. Distant metastases from head and neck squamous cell carcinoma. Part I. Basic aspects. *Oral Oncol*. 2012;48(9):775–779.
3. Nomura T, Shibahara T, Cui NH, Noma H. Patterns of mandibular invasion by gingival squamous cell carcinoma. *J Oral Maxillofac Surg*. 2005;63(10):1489–1493.
4. Ebrahimi A, Murali R, Gao K, Elliott MS, Clark JR. The prognostic and staging implications of bone invasion in oral squamous cell carcinoma. *Cancer*. 2011;117(19):4460–4467.
5. Vaassen LAA, Speel EM, Kessler PAWH. Bone invasion by oral squamous cell carcinoma: molecular alterations leading to osteoclastogenesis — a review of literature. *J Craniomaxillofac Surg*. 2017;45(9):1464–1471.
6. Cui N, et al. Osteoclast-related cytokines from biopsy specimens predict mandibular invasion by oral squamous cell carcinoma. *Exp Ther Med*. 2010;1(5):755–760.
7. Quan J, Johnson NW, Zhou G, Parsons PG, Boyle GM, Gao J. Potential molecular targets for inhibiting bone invasion by oral squamous cell carcinoma: a review of mechanisms. *Cancer Metastasis Rev*. 2012;31(1-2):209–219.
8. Qiao B, Johnson NW, Gao J. Epithelial-mesenchymal transition in oral squamous cell carcinoma triggered by transforming growth factor-beta1 is Snail family-dependent and correlates with matrix metalloproteinase-2 and -9 expressions. *Int J Oncol*. 2010;37(3):663–668.
9. Quan J, Elhousiny M, Johnson NW, Gao J. Transforming growth factor-β1 treatment of oral cancer induces epithelial-mesenchymal transition and promotes bone invasion via enhanced activity of osteoclasts. *Clin Exp Metastasis*. 2013;30(5):659–670.
10. Cannonier SA, Gonzales CB, Ely K, Guelcher SA, Sterling JA. Hedgehog and TGFβ signaling converge on Gli2 to control bony invasion and bone destruction in oral squamous cell carcinoma. *Oncotarget*. 2016;7(46):76062–76075.
11. Gerritsen ME, Peale FV, Wu T. Gene expression profiling in silico: relative expression of candidate angiogenesis associated genes in renal cell carcinomas. *Exp Nephrol*. 2002;10(2):114–119.
12. Borsig L, Wolf MJ, Roblek M, Lorentzen A, Heikenwalder M. Inflammatory chemokines and metastasis — tracing the accessory. *Oncogene*. 2014;33(25):3217–3224.
13. Itatani Y, et al. The role of chemokines in promoting colorectal cancer invasion/metastasis. *Int J Mol Sci*. 2016;17(5):E643.
14. Grassi F, Cristino S, Toneguzzi S, Piacentini A, Facchini A, Lisignoli G. CXCL12 chemokine up-regulates bone resorption and MMP-9 release by human osteoclasts: CXCL12 levels are increased in synovial and bone tissue of rheumatoid arthritis patients. *J Cell Physiol*. 2004;199(2):244–251.
15. Wright LM, Maloney W, Yu X, Kindle L, Collin-Osdoby P, Osdoby P. Stromal cell-derived factor-1 binding to its chemokine receptor CXCR4 on precursor cells promotes the chemotactic recruitment, development and survival of human osteoclasts. *Bone*. 2005;36(5):840–853.
16. Lee SK, et al. Human antigen R-regulated CCL20 contributes to osteolytic breast cancer bone

metastasis. *Sci Rep*. 2017;7(1):9610.
17. Kamalakar A, et al. Circulating interleukin-8 levels explain breast cancer osteolysis in mice and humans. *Bone*. 2014;61:176–185.
18. Palma BD, et al. Osteolytic lesions, cytogenetic features and bone marrow levels of cytokines and chemokines in multiple myeloma patients: role of chemokine (C-C motif) ligand 20. *Leukemia*. 2016;30(2):409–416.
19. Watanabe H, Iwase M, Ohashi M, Nagumo M. Role of interleukin-8 secreted from human oral squamous cell carcinoma cell lines. *Oral Oncol*. 2002;38(7):670–679.
20. Prasad G, McCullough M. Chemokines and cytokines as salivary biomarkers for the early diagnosis of oral cancer. *Int J Dent*. 2013;2013:813756.
21. Panda S, Padhiary SK, Routray S. Chemokines accentuating protumoral activities in oral cancer microenvironment possess an imperious stratagem for therapeutic resolutions. *Oral Oncol*. 2016;60:8–17.
22. Oue E, et al. CXCL2 synthesized by oral squamous cell carcinoma is involved in cancer-associated bone destruction. *Biochem Biophys Res Commun*. 2012;424(3):456–461.
23. Sambandam Y, Sundaram K, Liu A, Kirkwood KL, Ries WL, Reddy SV. CXCL13 activation of c-Myc induces RANK ligand expression in stromal/preosteoblast cells in the oral squamous cell carcinoma tumor-bone microenvironment. *Oncogene*. 2013;32(1):97–105.
24. Chang KP, et al. Serum levels of chemokine (C-X-C motif) ligand 9 (CXCL9) are associated with tumor progression and treatment outcome in patients with oral cavity squamous cell carcinoma. *Oral Oncol*. 2013;49(8):802–807.
25. Quan J, Morrison NA, Johnson NW, Gao J. MCP-1 as a potential target to inhibit the bone invasion by oral squamous cell carcinoma. *J Cell Biochem*. 2014;115(10):1787–1798.
26. Kim HJ, Park J, Lee SK, Kim KR, Park KK, Chung WY. Loss of RUNX3 expression promotes cancer-associated bone destruction by regulating CCL5, CCL19 and CXCL11 in non-small cell lung cancer. *J Pathol*. 2015;237(4):520–531.
27. Park J, et al. Loss of RUNX3 expression inhibits bone invasion of oral squamous cell carcinoma. *Oncotarget*. 2017;8(6):9079–9092.
28. Tsai JH, Yang J. Epithelial-mesenchymal plasticity in carcinoma metastasis. *Genes Dev*. 2013;27(20):2192–2206.
29. Buijs JT, Stayrook KR, Guise TA. TGF-β in the bone microenvironment: role in breast cancer metastases. *Cancer Microenviron*. 2011;4(3):261–281.
30. Yu H, Shen Y, Hong J, Xia Q, Zhou F, Liu X. The contribution of TGF-β in epithelial-mesenchymal transition (EMT): down-regulation of E-cadherin via snail. *Neoplasma*. 2015;62(1):1–15.
31. Xiong N, Fu Y, Hu S, Xia M, Yang J. CCR10 and its ligands in regulation of epithelial immunity and diseases. *Protein Cell*. 2012;3(8):571–580.
32. Tang XH, Gudas LJ. Retinoids, retinoic acid receptors, and cancer. *Annu Rev Pathol*. 2011;6:345–364.
33. Shilkaitis A, Green A, Christov K. Retinoids induce cellular senescence in breast cancer cells by RAR-β dependent and independent pathways: potential clinical implications (Review). *Int J Oncol*. 2015;47(1):35–42.
34. Connolly RM, Nguyen NK, Sukumar S. Molecular pathways: current role and future directions of the retinoic acid pathway in cancer prevention and treatment. *Clin Cancer Res*. 2013;19(7):1651–1659.
35. Claus R, Lübbert M. Epigenetic targets in hematopoietic malignancies. *Oncogene*. 2003;22(42):6489–6496.
36. Lippman SM, Sudbø J, Hong WK. Oral cancer prevention and the evolution of molecular-targeted drug development. *J Clin Oncol*. 2005;23(2):346–356.
37. Sirchia SM, et al. Endogenous reactivation of the RARβ2 tumor suppressor gene epigenetically silenced in breast cancer. *Cancer Res*. 2002;62(9):2455–2461.
38. Shin M, et al. The inhibition of RANKL/RANK signaling by osteoprotegerin suppresses bone invasion by oral squamous cell carcinoma cells. *Carcinogenesis*. 2011;32(11):1634–1640.
39. van 't Hof RJ. The calvarial injection assay. *Methods Mol Biol*. 2012;816:537–544.
40. Kejner AE, Burch MB, Sweeny L, Rosenthal EL. Bone morphogenetic protein 6 expression in oral cavity squamous cell cancer is associated with bone invasion. *Laryngoscope*. 2013;123(12):3061–3065.
41. Zhou WN, et al. RUNX3 plays a tumor suppressor role by inhibiting cell migration, invasion and angiogenesis in oral squamous cell carcinoma. *Oncol Rep*. 2017;38(4):2378–2386.
42. Seki S, et al. Prognostic value of podoplanin expression in oral squamous cell carcinoma — a regression model auxiliary to UICC classification. *Pathol Oncol Res*. 2014;20(3):521–528.
43. Hwang YS, et al. Insulin-like growth factor-II mRNA binding protein-3 and podoplanin expression are associated with bone invasion and prognosis in oral squamous cell carcinoma. *Arch Oral Biol*. 2016;69:25–32.
44. Subarnbhesaj A, et al. Roles of VEGF-Flt-1 signaling in malignant behaviors of oral squamous cell carcinoma. *PLoS One*. 2017;12(11):e0187092.
45. Hsu YP, et al. Serum markers of CYFRA 21-1 and C-reactive proteins in oral squamous cell carcinoma. *World J Surg Oncol*. 2015;13:253.
46. Takayama Y, Mori T, Nomura T, Shibahara T, Sakamoto M. Parathyroid-related protein plays a critical role in bone invasion by oral squamous cell carcinoma. *Int J Oncol*. 2010;36(6):1387–1394.
47. Mickanin CS, Bhatia U, Labow M. Identification of a novel beta-chemokine, MEC, down-regulated in primary breast tumors. *Int J Oncol*. 2001;18(5):939–944.
48. Dimberg J, Hugander A, Wågsäter D. Protein expression of the chemokine, CCL28, in human colorectal cancer. *Int J Oncol*. 2006;28(2):315–319.
49. Liu GX, Lan J, Sun Y, Hu YJ, Jiang GS. Expression of the chemokine CCL28 in pleomorphic adenoma and adenolymphoma of the human salivary glands. *Exp Ther Med*. 2012;4(1):65–69.
50. Muthuswamy RV, Sundström P, Börjesson L, Gustavsson B, Quiding-Järbrink M. Impaired migration of IgA-secreting cells to colon adenocarcinomas. *Cancer Immunol Immunother*. 2013;62(6):989–997.
51. Maghazachi AA, Sand KL, Al-Jaderi Z. Glatiramer acetate, dimethyl fumarate, and monomethyl fumarate upregulate the expression of ccr10 on the surface of natural killer cells and enhance their chemotaxis and cytotoxicity. *Front Immunol*. 2016;7:437.
52. Facciabene A, et al. Tumour hypoxia promotes tolerance and angiogenesis via CCL28 and T(reg) cells. *Nature*. 2011;475(7355):226–230.
53. Ren L, Yu Y, Wang L, Zhu Z, Lu R, Yao Z. Hypoxia-induced CCL28 promotes recruitment of regulatory T cells and tumor growth in liver cancer. *Oncotarget*. 2016;7(46):75763–75773.
54. Huang G, Tao L, Shen S, Chen L. Hypoxia induced CCL28 promotes angiogenesis in lung adenocarcinoma by targeting CCR3 on endothelial cells. *Sci Rep*. 2016;6:27152.
55. Yang XL, Liu KY, Lin FJ, Shi HM, Ou ZL. CCL28 promotes breast cancer growth and metastasis through MAPK-mediated cellular anti-apoptosis and pro-metastasis. *Oncol Rep*. 2017;38(3):1393–1401.
56. Zou HY, et al. A truncated splice variant of human lysyl oxidase-like 2 promotes migration and invasion in esophageal squamous cell carcinoma. *Int J Biochem Cell Biol*. 2016;75:85–98.
57. Gong DH, Chen YY, Ma D, Chen HY, Ding KF, Yu KD. Complicated prognostic values of CCL28 in breast cancer by subtype. *J Thorac Dis*. 2019;11(3):777–787.
58. Soprano DR, Qin P, Soprano KJ. Retinoic acid receptors and cancers. *Annu Rev Nutr*. 2004;24:201–221.
59. Wen G, Wang H, Zhong Z. Associations of RASSF1A, RARβ, and CDH1 promoter hypermethylation with oral cancer risk: a PRISMA-compliant meta-analysis. *Medicine (Baltimore)*. 2018;97(11):e9971.
60. Hayashi K, Yokozaki H, Naka K, Yasui W, Lotan R, Tahara E. Overexpression of retinoic acid receptor beta induces growth arrest and apoptosis in oral cancer cell lines. *Jpn J Cancer Res*. 2001;92(1):42–50.
61. Sun SY, Wan H, Yue P, Hong WK, Lotan R. Evidence that retinoic acid receptor beta induction by retinoids is important for tumor cell growth inhibition. *J Biol Chem*. 2000;275(22):17149–17153.
62. Wan H, Oridate N, Lotan D, Hong WK, Lotan R. Overexpression of retinoic acid receptor beta in head and neck squamous cell carcinoma cells increases their sensitivity to retinoid-induced suppression of squamous differentiation by retinoids. *Cancer Res*. 1999;59(14):3518–3526.
63. Liu JP, Wei HB, Zheng ZH, Guo WP, Fang JF. Celecoxib increases retinoid sensitivity in human colon cancer cell lines. *Cell Mol Biol Lett*. 2010;15(3):440–450.
64. Kou Y, et al. Berberine suppressed epithelial mesenchymal transition through cross-talk regulation of PI3K/AKT and RARα/RARβ in melanoma cells. *Biochem Biophys Res Commun*. 2016;479(2):290–296.
65. Spurling CC, Suhl JA, Boucher N, Nelson CE, Rosenberg DW, Giardina C. The short chain fatty acid butyrate induces promoter demethylation and reactivation of RARbeta2 in colon cancer cells. *Nutr Cancer*. 2008;60(5):692–702.
66. Khan MA, et al. (-)-Epigallocatechin-3-gallate reverses the expression of various

tumor-suppressor genes by inhibiting DNA methyltransferases and histone deacetylases in human cervical cancer cells. *Oncol Rep*. 2015;33(4):1976–1984.
67. Zhang X, Junior CR, Liu M, Li F, D'Silva NJ, Kirkwood KL. Oral squamous carcinoma cells secrete RANKL directly supporting osteolytic bone loss. *Oral Oncol*. 2013;49(2):119–128.
68. Hwang YS, Lee SK, Park KK, Chung WY. Secretion of IL-6 and IL-8 from lysophosphatidic acid-stimulated oral squamous cell carcinoma promotes osteoclastogenesis and bone resorption. *Oral Oncol*. 2012;48(1):40–48.
69. Lee EJ, et al. Characterization of newly established oral cancer cell lines derived from six squamous cell carcinoma and two muco-epidermoid carcinoma cells. *Exp Mol Med*. 2005;37(5):379–390.
70. Kim KR, Kim HJ, Lee SK, Ma GT, Park KK, Chung WY. 15-Deoxy-$\Delta^{12,14}$-prostaglandin J_2 inhibits osteolytic breast cancer bone metastasis and estrogen deficiency-induced bone loss. *PLoS One*. 2015;10(4):e0122764.
71. Sasportas LS, Gambhir SS. Imaging circulating tumor cells in freely moving awake small animals using a miniaturized intravital microscope. *PLoS One*. 2014;9(1):e86759.
72. Chen Y, Dokmanovic M, Stein WD, Ardecky RJ, Roninson IB. Agonist and antagonist of retinoic acid receptors cause similar changes in gene expression and induce senescence-like growth arrest in MCF-7 breast carcinoma cells. *Cancer Res*. 2006;66(17):8749–8761.